beta 2-Integrin Adhesion Regulates Dendritic Cell Epigenetic and Transcriptional Landscapes to Restrict Dendritic Cell Maturation and Tumor Rejection

Guenther, Carla

2021-11

Guenther , C , Faisal , I , Fusciello , M , Sokolova , M , Harjunpää , H , Ilander , M , Tallberg , R , Vartiainen , M K , Alon , R , Gonzalez-Granado , J-M , Cerullo , V & Fagerholm , S C 2021 , ' beta 2-Integrin Adhesion Regulates Dendritic Cell Epigenetic and Transcriptional Landscapes to Restrict Dendritic Cell Maturation and Tumor Rejection ' , Cancer immunology research , vol. 9 , no. 11 , pp. 1354-1369 . https://doi.org/10.1158/2326-6066.CIR-21-0094

http://hdl.handle.net/10138/351747
https://doi.org/10.1158/2326-6066.CIR-21-0094

unspecified
acceptedVersion

β2-integrin adhesion regulates dendritic cell epigenetic and transcriptional landscapes to restrict dendritic cell maturation and tumor rejection

Carla Guenther [a], Imrul Faisal[a,+], Manlio Fusciello [b,+], Maria Sokolova [c], Heidi Harjunpää [a], Mette Ilander [a], Robert Tallberg [a], Maria Kristina Vartiainen [c], Ronen Alon[f], Jose-Maria Gonzalez-Granado [d,e], Vincenzo Cerullo [b], Susanna Carola Fagerholm [a]*

a, Molecular and Integrative Biosciences Research Programme, Faculty of Biological and Environmental Sciences, University of Helsinki, 00790 Helsinki, Finland
b, Faculty of Pharmacy, University of Helsinki, 00790 Helsinki, Finland
c, Institute of Biotechnology, University of Helsinki, 00790 Helsinki, Finland
d, LamImSys Lab. Instituto de Investigación Hospital 12 de Octubre (imas12), 28041 Madrid, Spain.
e, Departamento de Fisiología. Facultad de Medicina. Universidad Autónoma de Madrid (UAM), 28029 Madrid, Spain.
f, Weizmann Institute of Science, Israel

*__Corresponding Author__: Susanna Carola Fagerholm; e-mail: susanna.fagerholm@helsinki.fi; mailing address: Molecular and Integrative Biosciences Research Programme, Faculty of Biological and Environmental Sciences, PB 56 (Viikinkaari 9), 00014 University of Helsinki, Finland; phone: +358504486894
+ shared second author

Running title: β2-integrins regulate DC maturation and tumor rejection

Keywords: dendritic cell, integrin, epigenetics, programming, immunotherapy

Conflict of Interests Statement: The authors declare no potential conflicts of interest

Funding: This study was funded by the Academy of Finland, by project grants to SF, as well as under the framework of E-Rare-3, Sigrid Juselius Foundation, University of Helsinki (HiLIFE), Liv och Hälsa Foundation (all to SF) as well as by the Magnus Ehrnrooth Foundation (to CG and SF). ERA-Net for Research on Rare Diseases E-RARE (the LADOMICS consortium) covers funding for both RA and SF. Furthermore, by Instituto de Salud Carlos III (ISCIII) (PI17/01395; PI20/00306; SNSI3 program) with co-funding from the European Regional Development Fund (ERDF) “A way to build Europe” (To JG). V.C. acknowledges the European Research Council under the Horizon 2020 framework, ERC-consolidator Grant (Agreement n. 681219), Jane and Aatos Erkko Foundation (Project n° 4705796), HiLIFE Fellow (project n° 797011004), Finnish Cancer Foundations (project N° 4706116) and Magnus Ehrnrooth Foundation (project N° 4706235). M.K.V. is funded by Academy of Finland, Jane and Aatos Erkko, Sigrid Juselius, and Finnish Cancer foundations, as well as Helsinki Institute of Life Science.

Synopsis: This study reveals that β2-integrin-mediated adhesive interactions contribute to shaping dendritic-cell (DC) programming. Disrupting β2-integrin adhesion switches DCs to a mature, migratory phenotype that enhances antitumor responses, opening new avenues for optimization of DC-based cancer immunotherapy.

Abstract

Dendritic cells (DCs), the classical antigen-presenting cells of the immune system, switch from an adhesive, phagocytic phenotype in tissues, to a mature, non-adhesive phenotype that enables migration to lymph nodes to activate T cells and initiate antitumor responses. Monocyte-derived DCs are used in cancer immunotherapy but their clinical efficacy is limited. Here, we show that cultured bone marrow–derived DCs (BM-DCs) expressing dysfunctional β2-integrin adhesion receptors displayed enhanced tumor rejection capabilities in B16.OVA and B16-F10 melanoma models. This was associated with an increased $CD8^+$ T-cell response. BM-DCs expressing dysfunctional β2-integrins or manipulated to disrupt integrin adhesion or integrin/actin/nuclear linkages, displayed spontaneous maturation in *ex vivo* cultures (increased costimulatory marker expression, IL-12 production and 3D migration capabilities). This spontaneous maturation was associated with an altered DC epigenetic/transcriptional profile, including a global increase in chromatin accessibility and H3K4me3/H3K27me3 histone methylation. Genome-wide analyses showed that H3K4me3-methylation was increased on DC maturation genes, such as *CD86, Il12*, *Ccr7* and *Fscn1*, and revealed a role for a transcription factor network involving Ikaros and RelA in the integrin-regulated phenotype of DCs. Manipulation of the integrin-regulated epigenetic landscape in wild type (WT) *ex vivo* cultured BM-DCs enhanced their functionality in tumor rejection *in vivo*. Thus, β2-integrin-mediated adhesion to the extracellular environment plays an important role in restricting DC maturation and antitumor responses through regulation of the cellular epigenetic and transcriptional landscape. Targeting β2-integrins could therefore be a new strategy to improve the performance of current DC-based cancer immunotherapies.

Introduction

Dendritic cells (DCs) are professional antigen presenting cells. After capturing antigen in peripheral tissues, they mature and migrate to lymph nodes. In lymph nodes, DCs present antigen to T cells resulting in T-cell activation. DCs therefore act at the crossroad of innate and adaptive immunity and are crucial for antitumor responses, which makes them promising anticancer agents. The only DC-based cancer therapy, sipuleucel-T (Provenge), was approved by the FDA for prostate cancer in 2010. Other DC-based immunotherapeutics have been tested in patients with for example malignant melanoma, prostate cancer, malignant glioma and renal cell cancer (1). DC-based immunotherapeutics show low toxicity and induce immune responses in at least half the treated patients. However, their clinical efficacy is less impressive, for a variety of reasons, including problems in the ability of injected DCs to migrate to lymph nodes (only about 1% of injected cells migrate) and in their T-cell activation and polarization capacity, which may not be optimal for antitumor responses (1). Therefore, although these therapies are promising, further development to optimize their functionality in patients is required.

DCs are broadly classified into conventional (or classical) cDCs and plasmacytoid pDCs, which have specialized functions in the immune system. Migratory DCs are DCs that have left their tissue of origin and migrated to lymph nodes to activate T cells. Broadly speaking, $CD103^+$ migratory cDC1 are essential for $CD8^+$ T-cell activation, whereas $CD11b^+$ migratory cDC2 are the most efficient at driving $CD4^+$ T-cell activation. DCs also migrate to lymph nodes in steady state, which is important for the induction of tolerance. Based on their transcriptional profile, granulocyte-macrophage colony-stimulating factor (GM-CSF)-cultured murine monocyte-derived DCs (moDCs) resemble *in vivo* migratory DCs, making them a useful *in vitro* tool to investigate migratory DC function (2), and resemble the human moDCs (derived in culture with GM-CSF and IL-4) that are used in the majority of immunotherapeutics tested in patients (3,4). The migratory phenotype of DCs is associated with increased expression of *Ccr7*, the chemokine receptor for CCL19/CCL21, which guides DCs to lymph nodes. Migratory DCs also express many other genes associated with cell migration, such as *Cd74* (5), *Arc/Arg3.1* (6) and *Fscn1* (7). However, the mechanisms mediating the transcriptional switch between the antigen capture phenotype of immature DCs and the migratory phenotype of mature DCs, remains to be unraveled.

We have previously reported that the mature, migratory phenotype of DCs is restricted by β2-integrins (8). β2-integrins are a family of heterodimeric adhesion receptors that share the common β2 chain, which is also known as CD18. The four members are αLβ2 (or CD11a/CD18), αMβ2 (or CD11b/CD18), αXβ2 (or CD11c/CD18) and αDβ2 (or CD11d/CD18). β2-integrins are expressed on leukocytes and are involved in many essential immunological processes that require cell adhesion to other cells, such as leukocyte adhesion under flow, immunological synapse formation and phagocytosis. β2-integrin-mediated adhesion is controlled by cytoplasmic factors such as talin and kindlin-3, which regulate integrin activation and ligand binding. A mutation of three threonines of the β2-integrin cytoplasmic domain (TTT/AAA β2-integrin knock-in [KI]) renders all β2-integrins inactive by significantly reducing the binding of kindlin-3 (9). We have previously shown that murine bone marrow–derived DCs (BM-DCs) expressing inactive integrins become reprogrammed to a mature, migratory phenotype, characterized by major transcriptional changes, increased surface expression of CD40, CD80, CD86 and CCR7, as well as increased cytokine production (IL-10, IL-12) (8). These results highlight β2-integrins as essential regulatory elements of the phenotypic switch of DCs to the mature, migratory phenotype, but the mechanisms mediating this cellular reprogramming have remained elusive.

In this study, using murine BM-DCs as a model system, we have discovered a β2-integrin adhesion-regulated mechanism that controls the DC phenotypic switch from the antigen capture phenotype to the mature, migratory phenotype. We found that β2-integrins regulate the DC epigenetic state (histone methylation) and transcriptional landscape through transcription factors (TFs) such as Ikaros and RelA. Furthermore, integrins restricted the expression of DC costimulatory molecules and cytokines, the cell's 3D migration speed and DC-mediated tumor rejection *in vivo*. External targeting of this integrin-regulated transcriptional program of DCs led to increased DC-mediated tumor rejection in two murine melanoma models *in vivo.* Our results highlight a new function of β2-integrin-mediated immune cell adhesion in regulating DC epigenetic and transcriptional programming, offering a potential target to optimize DC-based immunotherapy approaches in the future.

Materials and Methods

Mice and bone marrow collection

Integrin TTT/AAA β2-integrin knock-in mice (β2-integrin KI) have been previously described (9). WT littermates and male and female C57BL/6N mice purchased from Charles River and Scanbur were used as controls for Integrin TTT/AAA β2-integrin knock-in mice. C57BL/6-Lmna$^{flox/flox}$ mice were from Jackson (Jackson laboratory Stock No 026284) and were crossed with C57BL/6-LysM-CRE (Jackson laboratory Stock No 004781) to generate mice from which lamin A/C knockout (KO) moDCs could be generated, and littermates were used as controls. Bone marrow from CCR7$^{-/-}$ mice was kindly provided by Prof Reinhold Foerster. Experiments were performed using male and female mice between ages 8 and 39 weeks. Animals were housed under conventional conditions in groups of up to 5 animals per cage with free access to food and water. Bone marrow was collected from euthanized animals and used for BM-DC cultures immediately, except for Lamin and CCR7$^{-/-}$ for which the isolated bones where shipped to Finland and then bone marrow was isolated. For tumor experiments, C57BL/6J female mice were purchased from Scanbur. Mice were 8 weeks old when the experiments started. The experiments were performed according to the Finnish Act on Animal Experimentation (62/2006) and approved by the Finnish National Animal Experiment Board.

DC culture

DCs were generated by culturing bone marrow for 9–10 days in 10 ng/ml GM-CSF (Peprotech, cat. # AF-315-03) in DC media eg RPMI (Lonza, cat. #BE12-167F) +10% FCS, 100 U/ml penicillin-streptomycin (penicillin, Orion, cat. # 465161; streptomycin Thermo Fisher Scientific, cat. # D7253-100g) and 2 mM L-glutamine (Thermo Fisher Scientific, cat. # BP379-100), 37°C in a humidified atmosphere of 5 % CO_2. with media

addition/change on days 3, 6, and 8. In some experiments, cells were treated with Cytochalasin D (Cyto D) 10 µg/ml (Tocris, cat. # 1233), Tranylcypromine hydrochloride (TCP) 5µM (Tocris, cat. # 3852), Lenalidomide 10µM (Sigma, cat. # SML2283) 8-hydroxy-5-quinolinecarboxylic acid (IOX1) 5µM (Cayman, cat. # 11572), lipopolysaccharide (LPS) (100ng/ml, Sigma, cat. # L6529), bafilomycin (12,5 nM, Sigma, cat. # B1793) and MG132 (2,5 µM, Sigma, cat. # M7449), all overnight. For some experiments DCs were seeded on fibronectin (10µg/ml, Calbiochem, cat. # 86088-83-7) or coated cover slips overnight. For DC incubation in suspension, DCs were detached from plates by incubating cells in 5mM EDTA (Sigma, cat. # E5134-1kg) for 12 minutes and subsequently washing the cells off by pipetting up and down multiple times with 2% FCS/PBS, resuspended in DC media (described above) to $1x10^6$/ml and left in 50ml conical centrifuge tubes (Falcon™) with loose lid overnight.

Tumor models and cell lines

The murine melanoma cell line B16.F10 was purchased from the American Type Culture Collection (ATCC; Manassas, VA, USA) and the ovalbumin-expressing murine melanoma cell line B16.OVA was provided by Prof. Richard Vile (Mayo Clinic, Rochester, MN, USA). Both cell lines were genotyped in the beginning of the year. B16.OVA were used at a passage of 25 while B16F10 at a passage of 5. Mycoplasma test is routinely done after 1 week post culturing by analyzing the supernatant of the cells with MycoAlertTM Mycoplasma Detection Kit (Lonza, cat. #: LT07). Both cell lines were cultured in RPMI 1640 medium (Lonza, cat. # 12167F) containing 10 % FBS, 2 mM L-glutamine (Thermo Fisher Scientific, cat. # BP379-100), 1 % penicillin/streptavidin (penicillin, Orion cat. # 465161; streptomycin Thermo Fisher Scientific, cat. # D7253-100g). B16.OVA was cultured under Geneticin (Thermo Fisher Scientific, cat. # 10131035) selection at 37°C in a humidified atmosphere of 5 % CO_2. HL-60 transfected with a plasmid to overexpress lamin A/C along with controls transfected with ZsGreen1 retroviral vector were generated as previously described (10).HL-60 were provided by Ronen Alon in 2020, authentication and mycoplasma testing had been done in Ronen Alon's lab in 2017 and stored in liquid nitrogen until shipping. HL-60 were used at passage 8. Cells were maintained in RPMI +10% FCS, 20 mM HEPES, 100 U/ml penicillin-streptomycin and 2 mM L-glutamine (same vendors as DC culture), with media changes every three to four days. Two days prior to experiments, cells were differentiated into myeloid cells according to a previously published protocol, using 270 ng/ml A23187 (Chemcruz, cat. # sc-3591) (11,12).

Polyacrylamide gels with varying stiffness

In some experiments, cells were placed on polyacrylamide gels with different stiffness (Young's Moduli: 0,87kPa, 11kPa, 90kPa) (13) over night. Gels were coated with iC3b (6µg/ml; Calbiochem, cat. # 204863-250UG).

ELISA

The level of IL-12 from WT and KI BM-DC supernatants was assessed with Mouse IL-12/IL-23 p40 Allele-specific DuoSet ELISA kit according to the manufacturer's instructions (R&D, cat. # DY499). Briefly, a 96-well microplate was first coated with capture antibody overnight. The next day, the wells were washed and blocked with reagent diluent (1% BSA [Biowest, cat. # P6154] in PBS [Lonza, cat. # 17-516F]) for a minimum of one hour. The plate was then washed and standards and samples were added. Following a 2h incubation, the plate was washed and the detection antibody was added to the wells. After 2h, the plate was washed and Streptavidin-HRP was added for 20 min. After washing, substrate solution (R&D, cat. # DY499) was added to the wells. Following visible colour development (or latest after 20 min), sulphuric acid (Acros Organics, cat. # 124645001; diluted 1:4 in water) was added to stop the reaction. The optical density was immediately determined at 450 nm and background at 540 and 570 nm wave lengths using EnSpire fluorometer (Perkin Elmer). Background readings were subtracted from the readings at 450 nm and the sample IL-12 concentration was determined based on the standard curve. All steps were performed at room temperature.

All washing steps were performed by washing the plate first twice with 0,05% Tween (Fisher BioReagents, cat. # BP337) in PBS and then once with PBS only. The plate was covered from light during incubation with Streptavidin-HRP or substrate. All reagents were included in the kit DY499 unless stated otherwise.

Western blotting

Cells were lysed in M-PER lysis buffer (Thermo Fisher Scientific, cat. # 78501,) in the presence of phosphatase and protease inhibitors (Thermo Fisher Scientific, cat. # A32959), and lysates were analyzed by Western blotting. Primary antibodies against H3K4me3 (Cell Signaling Technology, cat. #9751S), and against H3K27me3 were from (Cell Signaling Technology, cat. #9733S).

Immunofluorescence staining and microscopy

$1x10^6$ DCs were seeded onto coverslips that were uncoated or coated with either fibronectin (10 µg/ml; Calbiochem, cat. # 86088-83-7) or fibrinogen (10µg/ml, Sigma, cat. # F-3879) on day 9, left RPMI (Lonza, cat. # BE12-167F) +10% FCS, 100 U/ml penicillin-streptomycin (penicillin, Orion, cat. # 465161; streptomycin, Thermo Fisher Scientific, cat. # D7253-100g) and 2 mM L-glutamine (Thermo Fisher Scientific, cat. # BP379-100) media overnight and fixed with 1% PFA. DCs incubated in suspension were left to adhere for 20 minutes before PFA fixation. Cells were permeabilized with 0.2% Triton-x in PBS for 5 minutes and stained for 1h at room temperature with the following antibodies diluted in 1%FBS/PBS according to the suppliers recommendations: H3K27me3 (Cell Signaling Technology, cat. # 9733S), H3K4me2 (Cell Signaling Technology, cat. # 9725T), H3K4me3 (Cell Signaling Technology, cat. # 9751S), RNA-polymerase II (phospho S2, Abcam cat. # ab5095), RelA (Santa Cruz, cat. # SC-8008), lamin A/C (Abcam, cat. # ab108922) and Lamin B (Santa Cruz, B-10, cat. # sc-374015). Cells were subsequently stained with an Alexa 594–conjugated anti-rabbit IgG (ThermoFisher Scientific, cat. # A-21207) or Alexa 555–conjugated anti-mouse IgG (ThermoFisher Scientific, cat. # A21422). Corrected total cell fluorescence (CTCF) values were calculated based on measurements of area, intensity and background with Image J as previously described (14). 25–100 cells per condition were measured for each animal. Nuclei were stained with DAPI (Sigma, cat. # D9542).

All slides were imaged using a Leica SP5 II (Leica Microsystems) LAS AF Lite Software using a sequential scan, with 561 Laser (10% laser power): 580–752 nm, Smart Gain 900 V, Smart Offset 0.0% for scan 1. Scan 2 was done with 405 Laser (10% laser power): 415–575 nm, Smart Gain 750 V, Smart Offset -1.0%. Z-stacks were taken with the following parameters: max QD405/488/561/635 mirror, Pinhole 111,39 µm, Zoom: 1,00; Objective 63X, z-volume 10,127 µm, 0,25µm step size, Line Average 3, Format 512x512.

DC flow cytometry

The following conjugated antibodies were used for flow cytometry of dendritic cells and HL-60, of at least 10000 whole cells (See Supplementary Fig 1 for gating strategies and Supplementary Fig 2 for representative histograms) (company, cat nr and clones given in brackets): CD11a-PE (BioLegend, cat. # 101008, clone 2D7), CD18-FITC (BD Biosciences, cat. # 553292, clone C71/16), CD11c-PE-Cy7 (eBioscience, cat. # 25-0114-81, clone N418), CD11b-APC (BioLegend, cat. # 17-0112-82, clone M1/70), MHCII- APC-eFluor780 (eBioscience, cat. # 47-5321-82, clone M5/114.15.2), CD80-APC (cat. # 17-0801-81, eBioscience, clone 16-10A1), CCR7-PE (cat. # 120106, BioLegend, clone 4B12), CD40-PE (cat. # 124609, BioLegend, clone 3/23), CD86-FITC (cat. # 11-0862-85, BD Biosciences, clone GL1). Fc block (cat. # 14-0161-86, eBiosciences, clone 93) was included in all stains. Isotype controls used were the following: FITC, BD Pharmingen, cat. # 556652; PE, BD Pharmingen, cat. # 556653; PE-Cy7, eBioscience, cat. # 25-4321-81; APC, eBioscience, cat. # 17-4888-81; APC-eFluor780, eBioscience, cat. # 47-4321-80). For analysis of DC and macrophage proportions, cells were first resuspended in FACS buffer containing anti-CD16/32 (BD Pharmingen, cat. # 553142, clone 2.4G2) to block Fc receptors. Cell surface staining was then performed using the following antibodies: MHC class (II I-A/I-E) APC-eFluor780 (eBiocience, cat. #47-5321-82, clone M5/114.15), CD11c AlexaFluor700 (eBioscience, cat. #56-0114-80, clone N418), CD11b FITC (eBioscience, cat. #11-0112-82, clone M1/70), CD115 APC (eBioscience, cat. #17-1152-80, clone AFS98), CD135 PE (eBioscience, cat. #12-1351-81, clone A2F10) and MerTK BV421 (BioLegend, cat.

#151510, clone 2B10C42). FMO controls were used for each fluorochrome and in addition, the following isotype controls were used: Armenian hamster IgG AlexaFluor700 (eBioscience, cat. #56-4888-80, clone eBio299Arm), Rat IgG2a kappa APC (eBioscience, cat. #17-4321-81, clone eBR2a), Rat IgG2a kappa PE (eBioscience, cat. #12-4321-80, clone eBR2a), Rat IgG2a kappa BV421 (Biolegend, cat. #400535, clone RTK2758). Propidium iodide (Sigma, cat. #P4864) was used to detect dead cells.

. Propidium iodide (Merck, cat. # P4864Merck) was used to detect dead cells.

Acquisition was performed on an LSR Fortessa flow cytometer (Becton Dickinson). Data were analyzed using FlowJo software (TreeStar, OR, USA).

Cell migration assays

3D migration assays were performed with µ-Slide Chemotaxis 3D (Ibidi, cat. # 80326) imaging slides according to the manufacturer's protocol. Briefly DCs were mixed into a bovine collagen I (CellSystems, cat. # 5005-B) mix and injected into the slide's thin imaging strip. After 45 minutes collagen polymerization, one of two chambers flanking the imaging strip was filled with DC media mentioned above, the other with media containing mCCL19 (R&D systems, cat. # 440-M3-025). One slide was used for each condition. DCs were imaged using 3I Marianas imaging system (3I intelligent Imaging Innovations, Germany) by utilizing multipoint imaging. Controls were always imaged before treated or knock-in/-out DCs. A 10x/0.30 EC Plan-Neofluar Ph1 WD=5.2 M27 objective was used, the dish was placed in a heated sample chamber (+37°C), in controlled 5 % CO_2 atmosphere. Cells were imaged using bright field microscopy. β2-integrin KI versus WT leukocyte migration was compared for 4h by cell tracking every 2 minutes (for all other analyses 1 min). For calculating the mean migration speed the velocities of only migratory DCs (defined as DCs that migrated faster than 1 µm/minute) were incorporated.

Chromatin immunoprecipitation (ChIP) assays

For ChIP, β2-integrin KI, WT, WT TCP and WT TCP+suspension DCs were fixed in 1% formaldehyde/PBS for 10 minutes at room temperature, crosslinking was stopped by adding glycine (Sigma, cat. # 50046) to a final concentration of 0.125 M for 5 minutes, followed by scraping adherent cells off the plates. Cell pellets of $10x10^6$ DCs per condition were lysed in 300 µl of RIPA buffer (Pierce, cat. # 89900) and sonicated with Bioruptor (Diagenode; number of cycles = 15, power = HIGH, ON = 30 seconds, OFF = 30 seconds). At least $3x10^6$ DCs were used per one IP. IPs were carried out with 5 µg antibody, H3K4me2 (Cell Signaling Technology, cat. #9725T, C64G9), H3K4me3 (Cell Signaling Technology, cat. #9751S, C42D8) overnight at 4°C in a rotating wheel. The immuno-complexes were collected with 50 µl of blocked protein A sepharose (GE Healthcare, cat. #17-0780-01) at 4 °C for two hours with rotation. The beads were pelleted by centrifugation at 4 °C for one minute at 500 G and washed sequentially for five minutes on rotation with 1 ml of the following buffers: low-salt wash buffer (RIPA) (10 mM Tris–HCl (pH 8.0), 0.1 % SDS, 1 % Triton X-100, 1 mM EDTA, 140 mM NaCl, 0,1 % sodium deoxycholate), high-salt wash buffer (10 mM Tris–HCl (pH 8.1), 0.1 % SDS, 1 % Triton X-100, 1 mM EDTA, 500 mM NaCl, 0,1 % sodium deoxycholate) and LiCl wash buffer (10 mM Tris–HCl (pH 8.1), 0.25 mM LiCl, 0,5 % IGEPAL CA-630, 0,5 % sodium deoxycholate, 1 mM EDTA). Finally, the beads were washed twice with 1 ml of TE buffer (10 mM Tris–HCl (pH 8.0), 1 mM EDTA). Chromatin was eluted in 150 µl of 1% SDS in TE buffer. The cross-linking was reversed by adding NaCl to final concentration of 200 mM and incubating at 65 °C overnight. The eluate was treated with Proteinase K (Sigma, cat. # P6556) and the DNA was recovered by extraction with phenol/chloroform/isoamylalcohol (25/24/1, Sigma cat. #77617) and precipitated with 0.1 volume of 3 M sodium acetate (pH 5.2) and two volumes of ethanol using glycogen as a carrier.

ChIP libraries were prepared for Illumina NextSeq 500 using NEBNext ChIP-Seq DNA Sample Prep Master Mix Set for Illumina (NEB, cat. # E6240) and NEBNext® Multiplex Oligos for Illumina® (Index Primers Set 1) (NEB, cat. #E7335) according to the manufacturer's protocols. Sequencing was performed with NextSeq500 at Biomedicum Functional Genomics Unit (FuGU), University of Helsinki. Sequencing was performed in

duplicate. ChIP-Seq data sets were aligned using Bowtie2 [using ChIPster software (15)] to version mm10 (GRC m38) of the mouse genome with the default settings. To visualize and present ChIPseq data, we used Integrative Genomics Viewer [IGV; (16)] and EaSeq (http://easeq.net) (17). Fastq files are deposited at NCBI's Gene Expression Omnibus (GEO) database with BioProject ID PRJNA599281 and BioSample accession number SAMN14687879.

Assay for Transposase-accessible chromatin (ATAC) seq

ATAC-Seq was performed according to the omni-ATAC protocol (18), which is a modified version of the protocol published in the original Buenrostro et al. papers (19,20). In the Omni-ATAC method, the composition of the cell lysis buffer and the transposition reaction buffer is modified to yield higher number of peaks and reduce mitochondrial reads. Briefly, 50,000 DCs were used for each reaction/sample and lysed for 3 minutes on ice using 50 µl cold ATAC-resuspension buffer (10 mM Tris-HCl, pH: 7.5, 10 mM NaCl, 3 mM MgCl2 in sterile water) containing 0.1% NP40, 0.1% Tween-20 and 0.01% Digitonin. The lysates were then washed with 1 ml cold ATAC-resuspension buffer containing only 0.1% Tween-20. Transposition mix (50 µl for each sample) was prepared using 25 µl 2x transposition buffer (Illumina, cat. #15027866), 2.5 µl Tn5 transposase enzyme (Illumina, cat. #15027865), 16.5 µl PBS, 0.5 µl 1% digitonin, 0.5 µl 10% Tween-20 and 5 µl sterile nuclease free H_2O. Pellet nuclei were resuspended in 50 µl transposition mix and incubated at 37 °C for 30 minutes on a thermomixer with mixing. These reactions were cleaned up using a PCR cleanup and concentrator kit (ThermoFisher Scientific GeneJET PCR purification kit, cat. #K0701) and eluted in 20 µl elution buffer. The eluted DNA was PCR amplified for 10 cycles using the following 50 µl PCR mix: 2.5 µl of each of the i5 and i7 index sequences (Illumina Nextera DNA CD Indexes, cat. #20015881), 25 µl NEBNext Ultra II Q5 Master Mix (cat. #M0544S) and 20 µl transposed samples. The PCR products were purified and size selected using AMPure XP beads (Beckman Coulter, cat. #A63880), the libraries were quantified using KAPA library quantification kit (KAPAbiosystems, cat. #07960140001). The size of the pooled library was examined by TapeStation. Paired-end (2x42 bp) sequencing was performed on Illumina NextSeq 500 at the Biomedicum Functional Genomics Unit (FuGU), University of Helsinki.

Paired reads were aligned to the mouse reference genome mm10 using STAR. PCR duplicates were removed using Picard followed by removal of mitochondrial reads. Peak-calling was performed using MACS2 with parameters --nomodel --shift -100 --extsize 200 --broad. Footprinting analysis on ATAC-seq data was performed using TOBIAS (Transcription factor Occupancy prediction By Investigation of ATAC-seq Signal) (21). TOBIAS is a comprehensive computational framework that is capable of handling Tn5 insertion bias correction, calculating footprint scores within regulatory regions and estimating bound and unbound TF binding sites. The Tn5 transposase inherent insertion bias was corrected using TOBIAS ATACorrect tool and footprinting scoring was performed using TOBIAS ScoreBigwig. TF binding across the genome of β2-integrin KI DCs and WT DCs was predicted by TOBIAS BINDetect. Fastq files are deposited at NCBI's Gene Expression Omnibus (GEO) database with BioProject ID PRJNA599281 and BioSample accession number SAMN13742355.

RNA-Sequencing

RNA-Sequencing library preparation and sequencing protocol was published previously (8). Here, the fastq raw files for all the three KI and three WT control samples were re-analyzed using the method below. After quality control performed by FastQC, sequencing reads fastq files were then aligned with HISAT2 alignment tool against the mouse reference genome (Mus musculus GRCm38.95). Transcripts were then counted per gene using a python package HTSeq. Differential expression analysis statistics was the performed by DESeq2. All genes having p-value <0.05 were considered as differentially expressed genes. Log2 fold change (log2FC) values, calculated by DESeq2, were indicator of upregulated (having positive log2FC values) and downregulated genes (having negative log2FC values).

Ikaros regulated genes are from (38), whereas PU.1 activated genes are listed from (34). Ikaros regulated genes were compared with all upregulated genes in KI DCs identified by our RNA-Seq analysis as described above. In contrast, PU.1 regulated genes were compared with only those genes in our RNA-Seq analysis which were at least two-fold upregulated in KI DCs. Common intersect genes were identified using R. GO-analyses of the intersect genes were perfomed by metascape (22). RelA bound (based on TLR-stimulation) in BMDCs were listed in (39), and were compared with all upregulated genes in the KI DCs RNA-Seq analysis.

TTRUST analysis Transcriptional Regulatory Relationships Unraveled by Sequence-based Text mining (TRRUST) is a manually curated database of human and mouse transcriptional regulatory networks. It uses sentence-based text mining approach. Currently, TRRUST contains 8,444 TF-target regulatory relationships of 800 human TFs, and 6,552 TF-target regulatory relationships for 828 mouse TFs. TRRUST version 2 was used here to identify active TFs associated with our genes of interest. The input gene list for this analysis was the common intersect 132 gene list of "Ikaros activated" and "upregulated in the KI".

qPCR

Total RNA was isolated from DCs with Nucleospin RNA kit (Macherey-Nagel, cat. #740955) and converted into cDNA by using High-Capacity cDNA Reverse Transcription kit (, Thermo Fisher Scientific, cat. # 4368814) according to the manufacturers' protocols. The quantitative Real-Time PCR (qRT-PCR) was performed by using Taqman chemistry. Briefly, the cDNA was amplified in 11 µl volume containing TaqMan Fast Advanced Master Mix (Thermo Fisher Scientific, cat. # 4444557) and TaqMan primers/probes (CCR7 Mm01301785_m1, Thermo Fisher Scientific). Each sample was run in triplicate, 18S rRNA (Thermo Fisher Scientific, cat. # 4333760T) was used as a reference gene and no template control (NTC) was included in the assay. Reactions were run with CFX96 Touch Real-Time PCR Detection System (Bio-Rad) and data analysed with CFX Maestro (Bio-Rad) and finalized with Excel (Microsoft). Relative units were calculated by using the comparative CT method.

Tumor experiments

Tumors were injected subcutaneously in the right flank (B16.OVA $3x10^5$ tumor cells/mouse and B16-F10 $1.5x10^5$ tumor cells/mouse) and grown until palpable. Mice were injected peritumorally with either 1 million β2-integrin KI DCs, WT DCs or PBS solution (MOCK). 8 mice per each condition were used. Tumor growth was followed with a caliper every second day. Caliper measurements were done on both sides of the tumor and the volume was calculated by the following formula: V=(Wx2xL), where W is tumor width and L is tumor length.

Immunophenotyping

To analyze the immune response systematically, blood, tumor and lymph node samples were immunophenotyped with flow cytometry. Peripheral blood (PB) was collected from the tail vein of mice before DC treatment and 4 days after. Red blood cells were lysed with ACK buffer (0.15 M NH_4Cl, 0.01 M $KHCO_3$, 0.1 mM EDTA). Tumors, spleens and draining lymph nodes were collected at the end point and cryopreserved at -80°C before assessing immune-cell content. See Supplementary Fig 1 for gating strategies and Supplementary Fig 2 for representative dot plots.

All samples were first resuspended in FACS buffer (2% FCS in PBS) containing anti-CD16/32 (BD Biosciences, cat. # 553142, either clone 93 or 2.4G2) to block Fc receptors. The following antibodies were used for the phenotyping of lymphocytes (company and clones given in brackets): CD45-PE-Cy7 (eBioscience, clone 30-F11, cat. # 25-0451-82) or CD45 BV650 (BD Biosciences, cat. # 563410, clone 30-F11), CD3e AlexaFluor488 (eBioscience, cat. # 53-0031-82, clone 145-2C11), CD4-PerCP (BD, cat. # 561090, clone RM4-5) or CD4 PE-Cy7

(Biolegend, cat. # 100528; clone RM4-5), CD8a-APC-Cy7 (BioLegend, cat. # 100713, clone 53-6.7), , CD69-APC (BioLegend, cat. # 104513, clone H1.2F3). Analysis of tumor-specific T-cell responses was done on samples taken on day 30 of the B16 OVA experiment: TruStain FcX™ anti-mouse CD16/32 (BioLegend, cat. # 101320), CD8-FITC (ProImmune, cat. # A502-3B-E), CD3e-PE (BD Pharmingen, cat. # 550353), CD19-PerCP (BioLegend, cat. # 115531). For intracellular staining (Tregs), cells were first surface stained and then fixed and permeabilized with Foxp3/Transcription Factor Staining Buffer Set (eBioscience, cat. # 00-5523-00) and stained with Foxp3 APC (eBiocience, cat. # 17-5773-80, clone FJK-16s). SIINFEKL epitope-specific T cells were studied using APC-labelled H-2Kb/SIINFEKL pentamer (ProImmune, cat. # F093-84B214 E). Samples were acquired with LSRFortessa (BD) and analysed with FlowJo (BD).

Statistical analysis

The Student's 2-tailed t-test and Mann-Whitney test, were used to calculate statistical significance in GraphPad Prism 6. For migration assays Mann-Whitney tests were used. For tumor growth experiments 2-way ANOVA was used. All p-values are shown as <0.05 *, <0.01 **, <0.005 ***, <0.0001 ****.

Results

Integrin inactivation increases DC maturation, migration and DC-mediated antitumor responses *in vivo*

We have previously shown that β2-integrins restrict the mature, migratory phenotype of DCs and DC-mediated T-cell activation and T helper cell (Th1) polarization *in vivo* (8,23). Here, we show that the β2-integrin TTT/AAA knock-in mutation, which inhibits the interaction between the integrin and its cytoplasmic regulator kindlin-3, resulting in expressed but inactive β2-family integrins, specifically resulted in significantly increased BM-DC surface expression of the costimulatory molecules CD40, CD80, CD86 and the chemokine receptor CCR7 (**Fig 1a**), but it did not affect macrophage/DC ratios in GM-CSF cultures (Supplementary Fig S3). Additionally, β2-integrin KI DCs produced increased amounts of IL-12 (p40) (**Fig 1b**) and migrated significantly faster than WT DCs in a 3D collagen matrix in the presence of CCL19 (**Fig 1c**). LPS-induced activation of WT DCs led to significantly higher levels of CD40, CD80 and CD86 expression and IL-12 production than were seen for nonactivated β2-integrin KI DC (Supplementary Fig 2h, 4a), although migration speed was higher for β2-integrin KI DCs than for LPS-stimulated WT DCs (Supplementary Fig 4b).

To further examine DC functionality *in vivo* we performed tumor rejection experiments with subcutaneously injected B16-OVA melanoma cells. After palpable tumors were established, unstimulated WT or β2-integrin KI DCs were injected peritumorally. Both β2-integrin KI and WT DCs initiated an antitumor response that controlled tumor growth, however β2-integrin KI DCs initiated a superior tumor rejection response (**Fig 1d**). There was a significant increase in OVA-specific $CD8^+$ T cells infiltrating tumors in mice injected with β2-integrin KI DCs compared with mice injected with WT DCs or MOCK DCs (**Fig 1e**). Additionally, mice injected with β2-integrin KI DCs had significantly increased OVA-specific $CD8^+$ T cells in the spleen and draining lymph nodes, demonstrating the systemic response to the tumor (OVA) protein (**Fig 1e**).

Subsequent analysis of immune cell populations in B16-F10 tumors (**Fig 1 f,g**) revealed significantly more activated $CD8^+$ T cells in the tumors of mice treated with β2-integrin KI DCs compared with mice treated with WT DCs (**Fig 1h, I**). There were similar amounts of $CD4^+$ T cells in the tumors of mice treated with β2-integrin KI DCs and those treated with MOCK (Supplementary Fig 5a). However, analysis of pooled tumor-draining lymph nodes showed an increase of $CD4^+$ T cells in mice that received β2-integrin KI DCs (Supplementary Fig 5b). In addition, there were significantly fewer $CD4^+$ T cells present in the blood stream in mice injected with β2-integrin KI DCs compared with mice that received WT DCs (Supplementary Fig 5c). Taken together, these results indicate that active β2-integrins restrict DC maturation and migration, and that DCs expressing inactive integrins induce increased tumor suppression *in vivo*, through an increased $CD8^+$ T-cell response.

Inactivating β2-integrins leads to an altered DC epigenetic state

We set out to investigate the molecular mechanism regulating DC maturation and migration downstream of β2-integrins. To identify regulatory pathways that could be responsible for the large gene expression changes in β2-integrin KI DCs compared with WT DCs that we previously reported (8) we analyzed histone methylation in WT and KI DCs. H3K4me3 is associated with active gene expression, whereas H3K27me3 is associated with repressed genes and heterochromatin formation; bivalent promoters carrying both marks usually characterize "poised" genes, ready to be switched on in specific cell types (26). We therefore analyzed global levels of both methylation marks in WT and β2-integrin KI DCs using immunofluorescence. We found that β2-integrin KI DCs had significantly increased intensity of both H3K4me3 and H3K27me3 compared with WT DCs (**Fig 2a-f**). In β2-integrin KI DCs H3K27me3 was present at the periphery of the nucleus (**Fig 2e**), which is characteristic for heterochromatin in most mammalian cells (27). Histone methylation changes in β2-integrin KI DCs were confirmed by Western blotting (**Fig 2g**). Also, TLR stimulation of DCs (with LPS) led to increased histone methylation (Supplementary Fig S6a, b). We also found increased phosphorylated Pol II staining in these cells, indicating increased gene transcription (**Fig 2h**).

Disrupting β2-integrin-mediated cell adhesion or the actin cytoskeleton results in DC maturation

We have shown that β2-integrins regulate the epigenetic state, phenotype and antitumor function of DCs. To investigate the role of cell adhesion in this process, we disrupted β2-integrin-mediated DC adhesion by detaching WT DCs from culture plates and incubating them in suspension overnight. This procedure resulted in upregulation of the costimulatory molecules CD40, CD80 and CD86 as well as increased IL-12 production (**Fig 3a, b** and (8)). We found that these phenotypic changes were accompanied by increased H3K4me3 and H3K27me3 levels (**Fig 3c**). Furthermore, we found that 3D migration speed in the presence of CCL19 was significantly increased for the first hour of the 3D migration assay **(Fig 3d**), but this was not sustained over the whole assay period (presumably because detached cells start adhering again to their environment).

In addition to β2-integrins (CD11a, CD11b, CD11c), murine BM-DCs also express β1-integrins and β3-integrins (28). However, neither adhesion of β2-integrin KI DCs to the β1-integrin ligand fibronectin nor to the β3-integrin ligand fibrinogen led to a reduction in histone methylation in these cells, showing that DC epigenetic state is regulated specifically by β2-integrins, and not generally by integrin-mediated cell adhesion (**Fig 3e,f**).

Integrins link to the actin cytoskeleton within cells, and we have previously reported that integrin/actin links are disrupted in β2-integrin KI DCs (8). Disrupting the actin cytoskeleton in WT DCs using cytochalasin D resulted in similar upregulation of costimulatory molecule expression as is seen in β2-integrin KI DCs (**Fig 3g, Fig 1a** and (8)). Cytochalasin D treatment also resulted in significantly increased levels of H3K4me3 and H3K27me3 in DCs (**Fig 3h**), indicating that β2-integrin/actin links regulate the epigenetic status of DCs. Overall, these results confirm that β2-integrin-mediated cell adhesion and β2-integrin/actin links regulate DC epigenetic state, maturation and migration.

β2-integrin/actin/lamin A/C crosstalk restricts histone methylation in DCs

Actin mechanically links integrin adhesion sites to the nucleus via the linker of nucleoskeleton and cytoskeleton (LINC) complex, which binds to the nuclear envelope composed of lamins (29). Lamins directly bind to DNA, specifically regions enriched with H3K9me2/3 and H3K27me3 (30). Furthermore, lamin A/C levels are regulated by mechanical stress, with cells on softer matrices having lower levels (31). We thus hypothesized that mechanical crosstalk between β2-integrins/kindlin-3/actin and nuclear lamins may physically regulate histone methylation state in DCs. Indeed, immunofluorescence staining of lamin A/C revealed a significant decrease of lamin A/C protein level in β2-integrin KI DCs compared with WT DCs (**Fig 3i**); lamin B levels were unchanged (**Fig 3j**). In addition, placing DCs on softer matrices coated with integrin ligands (and thereby reducing integrin-mediated mechanical stress in these cells) led to increased H3K4me3

levels (**Fig 3k**). Lamin A/C was not regulated at the transcriptional level in β2-integrin KI BM-DCs (**Fig 3l**). However, treating cells with the lysosomal inhibitor bafilomycin, but not the proteosomal inhibitor MG132, led to upregulation of lamin A/C protein levels in cells (**Fig 3m**), showing that DCs respond to changes in mechanical stress by lysosomal degradation of lamin, as has previously been reported in other cell types (32).

To directly investigate the role of this integrin/actin/lamin link in regulating the epigenetic status of DCs, we utilized lamin A/C KO DCs. These cells displayed significantly increased H3K4me3 and H3K27me3 levels (**Fig 3n**). However, lamin A/C KO DCs did not display increased costimulatory marker expression (Supplementary Fig S7a), elevated IL-12 (p40) production (Supplementary Fig S7b), or increased 3D migration speed (Supplementary Fig S7c). These results indicate that although lamin A/C absence in DCs results in changes of DC epigenetic status, lamin A/C absence alone is not enough to regulate the DC maturation status downstream of integrins when adhesion remains unchanged.

We hypothesized that by bypassing integrin-mediated mechanical signaling altogether, by increasing lamin levels in non-adhesive cells, it should be possible to modulate gene expression through this lamin-mediated epigenetic mechanism. Indeed, overexpressing lamin A/C in myeloid differentiated HL-60 cells led to significantly reduced CD80 and CCR7 expression in these cells (**Fig 3o, p**), confirming that modulating lamin A/C levels can regulate expression of particular costimulatory molecules in myeloid cells. However, as lamin A/C deletion in DCs on its own was not sufficient to induce DC phenotypical changes, altered gene expression and function in adhesive DCs may involve the recruitment of specific (integrin/actin-regulated) TFs downstream of integrin outside-in signaling.

Altered epigenetic landscape and chromatin accessibility in DCs expressing dysfunctional β2-integrins

To further investigate β2-integrin-mediated gene regulation on a global scale in an unbiased manner, we performed H3K4me3 ChIP-seq using WT and β2-integrin KI DCs. As is shown in **Fig 4a**, the mutation of the β2-integrin resulted in a global increase of methylation peak width compared with WT DCs. There was a significant overlap of H3K4me-tagged genes and genes that displayed increased expression in β2-integrin KI DCs (analyzed by RNA-seq analysis); 235 genes consistently displayed higher H3K4me3 around the transcription start site (TSS) in β2-integrin KI DCs than in WT DCs, and of these, 91 displayed increased RNA expression in β2-integrin KI cells (**Fig 4b**). Amongst these were genes associated with DC maturation and migration, including *Cd40*, *Cd80*, *Cd86*, *Il12b*, *Ccr7* and *Fscn1* (**Fig 4c-h**). H3K4me3 active histone methylation marks are therefore increased on a broad range of genes associated with the mature, migratory phenotype of β2-integrin KI DCs.

An Ikaros-regulated gene network drives the phenotype of β2-integrin KI migratory DCs

An altered epigenetic landscape in cells is associated with altered chromatin accessibility, enabling gene expression changes. To further investigate the role of β2-integrin-mediated chromatin regulation, we utilized ATAC-seq to map open chromatin regions in WT and β2-integrin KI DCs. Inactivating β2-integrins led to large-scale chromatin remodeling in DCs (Supplementary Fig S8S). Most ATAC-Seq enriched peaks in the β2-integrin KI DCs originated from promoter and intragenic regions of genes and they altogether scored around 70%, whereas intergenic peaks were also observed but at a lower portion (approximately 30% regions). Overall ATAC-Seq peaks around TSS and immediate downstream sequences were higher in the β2-integrin KI DCs (Supplementary Fig S8).

We next sought to identify putative TF-binding sites in the accessible chromatin regions that may be responsible for driving gene expression changes associated with the mature, migratory phenotype of DCs with dysfunctional β2-integrins. We analyzed ATAC-Seq peaks using TOBIAS ~~(Transcription factor Occupancy prediction By Investigation of ATAC-seq Signal), a comprehensive computational framework that is capable of handling Tn5 insertion bias correction, calculating footprint scores within regulatory regions and~~

~~estimating bound and unbound TF binding sites (21)~~. TOBIAS analysis identified several families of TFs enriched in β2-integrin KI DCs. The top 5 scoring TFs based on binding occupancy in β2-integrin KI DCs are shown in **Table 1**. Amongst these, Ikaros (encoded by the *Ikzf1* gene) binding sites were the most frequent, PU.1 (encoded by the *Spi1* gene) also scored highly. Ikaros is important for pDC development (33,34), and overexpression of PU.1 directs stem and lymphoid progenitor cells towards the myeloid lineage (35). PU.1 is also essential for defining the cDC lineage (35), and Ikaros/PU.1 interactions are involved in regulation of myeloid genes (36). Ikaros-activated gene targets that overlap with β2-integrin KI upregulated gene expression profiles are shown in **Fig 5a**. Genes activated by Ikaros and upregulated in β2-integrin KI DCs included important genes involved in DC-mediated regulation of T-cell activation and DC migration, such as *Ccr7, Cd86,* and *Il12b* (Supplementary Table 1). Next, we compared PU.1-regulated genes with the RNA-Seq upregulated genes in β2-integrin KI DCs. We found that 170 genes upregulated in the β2-integrin KI DCs were also activated by PU.1, and 100 of them were at least 2-fold upregulated (**Fig 5b**). This list of 100 genes contained important genes involved in DC migratory and inflammatory phenotypes (Supplementary Table 1). Overall, our data support the presence of an Ikaros/PU.1-regulated gene network which controls the transcriptional changes in mature, migratory DCs deficient in β2-integrin adhesiveness.

As the Ikaros TF cluster was the top scoring TF in our bioinformatic analyses (TOBIAS), we next investigated the role of Ikaros in regulating the β2-integrin KI DC phenotype. We found that lenalidomide (a cancer drug that leads to selective proteasome-induced degradation of Ikaros TFs (37)), significantly reduced IL-12 (p40) production in β2-integrin KI DCs (**Fig 5c**). In addition, lenalidomide treatment led to significantly reduced β2-integrin KI DC migration speed *in vitro* (**Fig 5d**). These results support the conclusion that Ikaros-family TFs play a major role in regulating the mature migratory phenotype of DCs downstream of β2-integrin adhesion.

A mechanically regulated Ikaros/NF-κB network in DCs

Our TOBIAS analysis identified an Ikaros TF network regulated by β2-integrins in DCs. However, RNAseq analysis (Supplementary Table 2) indicated that *Ikzf1* mRNA levels were not upregulated in β2 integrin KI cells (although mRNA levels of *Ikzf3* and *Ikzf4* were upregulated), raising the question of how loss of β2-integrin-mediated adhesion might activate the Ikaros TF network in β2-integrin KI DCs. TF network analysis showed connections between Ikaros and several other TFs including the NF-κB family members NFKB1, REL and RelA (Supplementary Fig S9). NF-κB signaling has previously been implicated as critical for the homeostatic DC migratory phenotype, although the upstream regulators of this pathway have not been identified (38). We have previously shown LPS-induced NF-κB signaling to be upregulated in β2-integrin KI DCs (8). Furthermore, RelA works together with Ikaros to regulate late gene expression in LPS-stimulated macrophages (39), with Ikaros leading to opening up of chromatin allowing for increased RelA binding at the same sites (39). We therefore compared our β2-integrin KI DC RNAseq dataset with validated RelA targets (ChIP-seq) from TLR-matured DCs (40). The results show that genes upregulated in the β2-integrin KI dataset were highly enriched for validated RelA binding sites (1076 sites) (**Fig 5e**). To further elucidate TF-target interactions, we used TRRUST (Transcriptional Regulatory Relationships Unraveled by Sentence-based Text mining) (41). TRRUST analysis of overlapping Ikaros-activated and β2-integrin KI upregulated genes indicated that the top TF regulating this group of genes was NF-κB, with RelA in third place (Supplementary Table 3). TRRUST database also lists REL, RELA, and NFκB1 among the TFs that share common targets with Ikaros. We therefore investigated whether NF-κB signaling was regulated by β2-integrin adhesion. Indeed, we found that RelA nuclear localization was significantly upregulated in β2-integrin KI DCs and nonadherent WT DCs detached from their adhesive substrate (**Fig 5f, g**). Furthermore, in WT DCs placed on soft matrices (**Fig 5h, i**), RelA displayed significantly increased nuclear localization compared with cells on stiffer matrix, which correlates with increased H3K4me3 staining in cells cultured on softer matrices (**Fig 4**). In addition, on very stiff surfaces, laminA/C KO DCs displayed significantly increased RelA nuclear localization compared with WT DCs (**Fig 5i**, 90kPa gels), indicating that a loss of laminA/C facilitates nuclear translocation of RelA particularly on stiffer

substrates. Together, these results show that RelA translocation into the nucleus is regulated at least in part by mechanotransduction through the integrin/lamin axis, and identify RelA as one of the TFs in the Ikaros TF network that accounts for the β2-integrin KI DC phenotype.

Taken together, our results show that β2-integrin-mediated adhesion is functionally coupled to an Ikaros/RelA-regulated transcriptional network. This network regulates the epigenetic status, gene expression landscape and mature, migratory phenotype of DCs, allowing DCs to respond to and functionally adapt to their tissue environment through β2-integrin-mediated cues.

Targeting integrin-regulated epigenetic changes increases DC migration and antitumor responses *in vivo*

Our result show that β2-integrins regulate epigenetic status and DC phenotype, and that blocking cell adhesion by cell detachment from culture plates leads to a transient increase in DC maturation, migration and H3K4me3 histone methylation. We reasoned that this phenotype may be transient (as seen in the cell migration assay), as cell reattachment may reverse the phenotype. We further reasoned that it may be possible to stabilize the adhesion-regulated epigenetic profile of DCs by directly targeting histone methylation in detached WT DCs. Therefore, we targeted H3K4 methylation directly by inhibiting lysine-specific demethylase 1 (LSD1) using TCP. We expected that this treatment should increase H3K4me2/3 levels, based on previous studies (42). TCP treatment indeed resulted in increased H3K4me2/H3K4me3 histone methylation on *Ccr7* (**Fig 6a**), but not on other genes that were upregulated in β2-integrin KI DCs (e.g. *Cd86*). Correspondingly, *Ccr7* mRNA level were significantly increased following combination treatment of TCP+suspension (**Fig 6b**).

We next investigated whether TCP treatment stabilized the mature, migratory phenotype of detached WT DCs. TCP treatment alone did not result in increased costimulatory molecule expression, however combining TCP treatment with suspension resulted in increased CD86 expression in DCs (**Fig 6c**). Likewise, IL-12 (p40) production was not increased in response to TCP treatment alone but was increased in response to combination treatment (**Fig 6d**). However, TCP treatment alone was sufficient to increase the 3D migration speed of DCs in response to the CCR7 ligand CCL19 (**Fig 6e**). Similar results were achieved with another histone demethylase inhibitor, IOX (**Fig 6f**), further strengthening our findings. Furthermore, combination-treated $CCR7^{-/-}$ DCs displayed reduced migration speed (**Fig 6g**), showing that migration was CCR7-dependent.

Finally, we investigated whether targeting the β2-integrin-regulated epigenetic changes in DCs would affect DC-mediated tumor rejection *in vivo* (**Fig 6h**). Injection of TCP+suspension-treated WT DCs into tumor-bearing mice resulted in a reduction of tumor growth that was very similar to that mediated by β2-integrin KI DC-treated mice, with $CD4^+$ T-cell recruitment into tumors, and reduced Treg numbers in tumors (Supplementary Fig S10). Experiments with TCP+suspension-treated $CCR7^{-/-}$ DCs showed that this increased tumor rejection was completely dependent on the chemokine receptor, presumably because it is required for DC trafficking from the tumor vicinity to the lymph nodes to induce T-cell activation (**Fig 6i**).

In conclusion, we have shown that β2-integrin-dependent adhesions connect to the nucleus via actin and the main nuclear lamina adaptor lamin A/C, thereby regulating the epigenetic landscape in DCs. Furthermore, integrins mechanically regulate RelA nuclear translocation, an Ikaros/NFkB TF network, chromatin accessibility and the gene expression profile of DCs. β2-integrin-mediated mechanosignaling thereby restricts excessive immune responses, primarily by suppressing the mature, migratory phenotype of DCs and DC-mediated T-cell activation, resulting in attenuated anti-tumor responses *in vivo.*

Discussion

Many cell types respond not only to biochemical cues but also to mechanical cues, such as tissue stiffness, shear flow and stretching, and these (and other) cues can together influence gene expression programs and cell fate . Immune cells such as DCs constantly traffic between tissues (peripheral tissues, lymphatics, lymph nodes) with different mechanical properties, which could potentially influence their functions. However, it is currently poorly understood how cell adhesion and mechanical cues sensed by distinct tissue leukocytes, and in particular DCs, shape immune cell gene expression profiles and thus, their cellular functions, although it has been previously reported that disrupting physical interactions of DCs can strongly induce their activation (43).

Integrins play major roles in mechanotransduction because they mediate adhesion to other cells and extracellular ligands, sense stiffness and transmit mechanical information into cells through signaling pathways, but also through direct mechanical links through their intracellular tails, via actin to the cell nucleus and chromatin (through the LINC (Sun/nesprin) complex and nuclear lamins (44)). This is linked to gene tethering to the nuclear envelope which correlates with tissue-specific gene suppression (45). When cells such as fibroblasts are cultured on stiff matrices, they display increased integrin-mediated cell adhesion, and the tension is transmitted through the integrin cytoplasmic domains ("tails"), through the cytoskeleton to the nucleus, where it can impact directly on chromatin organization. In contrast, cells on softer matrices display reduced adhesion and downregulation of lamin A/C, which can also have an impact on chromatin structure. β2-integrins, which are adhesion receptors abundantly expressed by all immune cells, therefore potentially have the ability to mechanically connect the extracellular environment of the cell to the nucleus to directly influence gene expression through several mechanisms, although these processes have not been extensively studied in immune cells.

In addition to their important roles in immune cell trafficking and activation, β2-integrins have been reported to restrict myeloid cell signalling and responses in many different settings. β2-integrins can inhibit TLR signalling in macrophages, promote tolerance and suppress inflammation, consistent with homeostatic and regulatory roles of these receptors in immunity and inflammation (46-53). Furthermore, we have previously shown that β2-integrins play a key role in regulating DC gene expression, and that β2-integrins inhibit DC maturation, migration to lymph nodes and DC-mediated Th1 polarization *in vivo* (48,54). In addition, we have discovered a β2-integrin-actin-MRTF-A/SRF pathway that regulates cell adhesion, traction force generation and cytoskeletal gene expression in DCs (55). However, this pathway regulates only a small subset of the genes affected by the β2-integrin KI-mutation, and is not involved in regulating DC 3D migration. Therefore, exactly how β2-integrin-mediated adhesion restricts immune cell function has remained poorly understood.

Here we show that β2-integrin-mediated adhesion to the extracellular environment regulates chromatin structure and the epigenetic landscape of DCs (e.g. histone methylation), and therefore DC gene transcription, maturation, migration and function *in vitro* and *in vivo*. These conclusions are based on our observations that a) disrupting DC adhesion by transferring them to suspension; b) interrupting the cytoskeletal associations of their β2-integrins; c) interfering with their actin cytoskeleton; d) deleting lamin A/C; and e) culturing DCs on softer matrices, drive similar global changes in histone methylation, providing evidence of mechanical regulation of the DC epigenetic landscape by β2-integrin-mediated adhesion.

We found that open chromatin regions in β2-integrin KI DCs are enriched with binding sites for Ikaros and other TFs such as PU.1. Our motif discovery analysis (known and de novo) identified Ikaros as the most significant TF in β2-integrin KI enriched ATAC-Seq peaks, suggesting that these TFs directly contribute to the mature migratory phenotype of these DCs. Indeed, our functional assays identified Ikaros as a main regulator of the β2-integrin KI DC phenotype. Ikaros/RelA are known to co-operate in regulation of gene transcription in myeloid cells (39), and our results further implicate RelA as an β2-integrin-regulated factor in this Ikaros transcriptional network. We therefore hypothesize that β2-integrin-mediated regulation of NF-κB signaling

provides at least one link between integrins and the Ikaros gene network that regulates DC phenotype and function. However, other mechanisms involved in β2-integrin-mediated regulation of the Ikaros gene network in these cells should be also considered, for example direct regulation of Ikaros complex through β2-integrin-regulated signaling pathways.

Based on our results, we propose that β2-integrin-mediated adhesion to the extracellular environment restricts DC programming to the mature, migratory phenotype by regulating the DC epigenetic/chromatin landscape. β2-Integrin-mediated adhesion regulates DC programming through β2-integrin/actin/chromatin crosstalk, affecting histone methylation status and chromatin accessibility. In addition, β2-integrins regulate transcription factor networks including Ikaros and RelA, further impacting on gene transcription programs in these cells. We propose that β2-integrin-mediated regulation can be used to fine-tune gene expression programs in these cells in response to the mechanical properties of the environment, in particular the stiffness of the interstitial space, which is controlled by collagen composition, density and crosslinking (56). Furthermore, after detaching from their environment in peripheral tissues, DCs interact with other cells and structures, such as lymphatic endothelial cells, and travel through the lymphatic system to lymph nodes. Such mechanical interactions could potentially confer DCs with a "mechanical memory" of the environments they engage and travel through. This memory of their integrated interactions with the extracellular matrix and with other cells, together with the biochemical cues they encounter, will determine DC location, function and survival.

However, in addition to conferring cells with an ability to adhere to the environment and sense extracellular mechanical properties, β2-integrins have the ability to be switched on, when adhesion is needed, and switched off, when it is not. Therefore, we propose that β2-integrins may also provide cells with a mechanism of "erasing" their mechanical memory, for example when a more pressing, overriding chemotactic or other stimulatory signal is encountered (such as during bacterial infection). Indeed, DCs downregulate β2-integrins and other cell adhesion receptors during maturation in both homeostatic and inflammatory settings (57,58), and the loss of β2-integrin adhesion in these cells contributes to the transcriptional changes associated with these switches. These large-scale transcriptional changes associated with epigenetic programming of the mature phenotype of DCs, dramatically enhance T cell activation and tumor infiltration of activated T cells *in vivo*.

A striking reflection of this concept of β2-integrin-dependent DC memory is the phenotype of adhesion-deficient DCs, which become reprogrammed to the mature, migratory phenotype, and induce better DC-mediated tumor rejection in two different melanoma models. Furthermore, by pharmacologically targeting this β2-integrin-regulated epigenetic reprograming in DCs, we could confer enhanced tumor-rejecting capabilities to WT DCs. Our study demonstrates that a central β2-integrin-mediated mechanism can be externally targeted to optimize DC- and T-cell mediated tumor control *in vivo*, although its relevance in human DCs require further studies. Nevertheless, these and other approaches to directly target β2-integrins and their cytoskeletal adaptors may be potentially promising means to optimize immunotherapy approaches in the future.

Authorship Contributions

SF planned the study. **CG** performed the experiments and analyzed results as far as not otherwise indicated. **IF** carried out ATAC seq experiment as well as RNA seq, ATAC seq and partial ChIP-seq data analyses, and further bioinformatics analyses. **MF** performed tumour experiments with help from **MI**, **RT** and **CG**. **MF** also performed immunophenotyping of T cell response. **MI** performed tumour phenotyping and analysis for first B16.OVA and B16-F10 experiment. **MS** taught and supervised sample generation for ChIP-seq and analysed ChIP-sequencing data. **HH** performed qPCR and analyzed qPCR results together with CG, and performed

tumor phenotyping and analysis for the TCP B16.OVA experiment and DC differentiation experiment and analysis. **MV** provided chemicals and covered the costs for the first ChIP-seq experiment. **VC** planned and covered the costs for the tumour experiments. **JG** provided lamin knockout and control mice. **RA** provided lamin overexpressing cells. **CG** wrote the paper together with **SF** and **IF**, and all others commented on the manuscript.

Acknowledgments

Virginia Zorita (Centro Nacional de Investigaciones Cardiovasculares Carlos III (CNIC), 28029 Madrid, Spain) is acknowledged for her help with tissue processing. Sara W Feigelson (Weizmann Institute of Science, Israel) is acknowledged for her help with shipments of the HL-60 cell variants. Reinhold Förster is acknowledged for kindly providing bone marrow from CCR7$^{-/-}$ mice.

Funding

This study was funded by the Academy of Finland, by project grants to SF, as well as under the framework of E-Rare-3, Sigrid Juselius Foundation, University of Helsinki (HiLIFE), Liv och Hälsa Foundation (all to SF) as well as by the Magnus Ehrnrooth Foundation (to CG and SF) and the the ERA-Net for Research on Rare Diseases E-RARE (the LADOMICS consortium) (to RA and SF) Furthermore, by Instituto de Salud Carlos III (ISCIII) (PI17/01395; PI20/00306; SNSI3 program) with co-funding from the European Regional Development Fund
(ERDF) "A way to build Europe" (To JG). V.C. acknowledges the European Research Council under the Horizon 2020 framework, ERC-consolidator Grant (Agreement n. 681219), Jane and Aatos Erkko Foundation (Project n° 4705796), HiLIFE Fellow (project n° 797011004), Finnish Cance Foundations (project N° 4706116), Magnus Ehrnrooth Foundation (project N° 4706235). M.K.V. is funded by Academy of Finland, Jane and Aatos Erkko, Sigrid Juselius, and Finnish Cancer foundations, as well as Helsinki Institute of Life Science.

Conflict of Interest Disclosures

The authors declare no competing financial interests.

References

1. Anguille S, Smits EL, Lion E, van Tendeloo VF, Berneman ZN. Clinical use of dendritic cells for cancer therapy. The Lancet Oncology **2014**;15(7):e257-67 doi 10.1016/S1470-2045(13)70585-0.
2. Helft J, Böttcher J, Chakravarty P, Zelenay S, Huotari J, Schraml BU*, et al.* GM-CSF Mouse Bone Marrow Cultures Comprise a Heterogeneous Population of CD11c+MHCII+ Macrophages and Dendritic Cells. Immunity **2015**;42:1197-211 doi 10.1016/j.immuni.2015.05.018.
3. Sallusto F, Lanzavecchia A. Efficient presentation of soluble antigen by cultured human dendritic cells is maintained by granulocyte/macrophage colony-stimulating factor plus interleukin 4 and downregulated by tumor necrosis factor alpha Journal of Experimental Medicine **1994**;179(4):1109-18 doi 10.1084/jem.179.4.1109. .
4. Huber A, Dammeijer F, Aerts JGJV, Vroman H. Current State of Dendritic Cell-Based Immunotherapy: Opportunities for in vitro Antigen Loading of Different DC Subsets? **2018**;9(2804) doi 10.3389/fimmu.2018.02804.
5. Faure-André G, Vargas P, Yuseff M-I, Heuzé M, Diaz J, Lankar D*, et al.* Regulation of dendritic cell migration by CD74, the MHC class II-associated invariant chain. Science **2008**;322(5908):1705-10 doi 10.1126/science.1159894.
6. Ufer F, Vargas P, Engler JB, Tintelnot J, Schattling B, Winkler H*, et al.* Arc/Arg3.1 governs inflammatory dendritic cell migration from the skin and thereby controls T cell activation. Science Immunology **2016**;1(3) doi 10.1126/sciimmunol.aaf8665.

7. Yamakita Y, Matsumura F, Lipscomb MW, Chou P-c, Werlen G, Burkhardt JK*, et al.* Fascin1 Promotes Cell Migration of Mature Dendritic Cells. The Journal of Immunology **2011**;186:2850-9 doi 10.4049/jimmunol.1001667.
8. Morrison VL, James MJ, Grzes K, Cook P, Glass DG, Savinko T*, et al.* Loss of beta2-integrin-mediated cytoskeletal linkage reprograms dendritic cells to a mature migratory phenotype. Nature Communication **2014**;5 doi 10.1038/ncomms6359.
9. Morrison VL, MacPherson M, Savinko T, Lek HS, Prescott A, Fagerholm SC. The β2 integrin–kindlin-3 interaction is essential for T-cell homing but dispensable for T-cell activation in vivo. Blood **2013**;122(8):1428–36. doi 10.1182/blood-2013-02-484998.
10. Yadav SK, Feigelson SW, Roncato F, Antman-Passig M, Shefi O, Lammerding J*, et al.* Elevated nuclear lamin A is permissive for granulocyte transendothelial migration but not for motility through collagen I barriers. Journal of Leukocyte Biology **2018**;104(2):239-51 doi 10.1002/JLB.3HI1217-488R.
11. Guo Q, Zhang L, Li F, Jiang G. The plasticity and potential of leukemia cell lines to differentiate into dendritic cells. Oncology Letters **2012**;4(4):595-600 doi 10.3892/ol.2012.821.
12. Li Q, Ozer H, Lindner I, Lee KP, Kharfan-Dabaja MA. Protein kinase C blockade inhibits differentiation of myeloid blasts into dendritic cells by calcium ionophore A23187 International Journal of Hematology **2005**;81(2):131-7 doi 10.1532/ijh97.na0405. .
13. Dembo M, Wang Y-L. Stresses at the Cell-to-Substrate Interface during Locomotion of Fibroblasts. Biophysical Journal **1999**;76(4):2307-16 doi 10.1016/S0006-3495(99)77386-8.
14. Abashidze A, Gold V, Anavi Y, Greenspan H, Weil M. Involvement of IKAP in Peripheral Target Innervation and in Specific JNK and NGF Signaling in Developing PNS Neurons. PLOS ONE **2014**;9(11) doi 10.1371/journal.pone.0113428.
15. Kallio MA, Tuimala JT, Hupponen T, Klemelä P, Gentile M, Scheinin I*, et al.* Chipster: user-friendly analysis software for microarray and other high-throughput data. BMC Genomics **2011**;12(507).
16. Robinson JT, Thorvaldsdóttir H, Winckler W, Guttman M, Lander ES, Getz G*, et al.* Integrative genomics viewer. nature biotechnology **2011**;29(1):24-6.
17. Lerdrup M, Johansen JV, Agrawal-Singh S, Hansen K. An interactive environment for agile analysis and visualization of ChIP-sequencing data. nature structural & molecular biology **2016**;23(4):349-57.
18. Corces MR, Trevino AE, Hamilton EG, Greenside PG, Sinnott-Armstrong NA, Vesuna S*, et al.* An improved ATAC-seq protocol reduces background and enables interrogation of frozen tissues. nature methods **2017**;14:959-62 doi 10.1038/nmeth.4396.
19. Buenrostro J, Wu B, Chang H, Greenleaf W. ATAC-seq: A Method for Assaying Chromatin Accessibility Genome-Wide. Current Protocols in Molecular Biology **2015**;109(1):21.9.1-.9.9 doi 10.1002/0471142727.mb2129s109.
20. Buenrostro JD, Giresi PG, Zaba LC, Chang HY, Greenleaf WJ. Transposition of native chromatin for fast and sensitive epigenomic profiling of open chromatin, DNA-binding proteins and nucleosome position. nature methods **2013**;10:1213–8 doi 10.1038/nmeth.2688.
21. Bentsen M, Goymann P, Schultheis H, Klee K, Petrova A, Wiegandt R*, et al.* ATAC-seq footprinting unravels kinetics of transcription factor binding during zygotic genome activation. nature communications **2020**;11(4267) doi 10.1038/s41467-020-18035-1.
22. Zhou Y, Zhou B, Pache L, Chang M, Khodabakhshi AH, Tanaseichuk O*, et al.* Metascape provides a biologist-oriented resource for the analysis of systems-level datasets. Nature Communications **2019**;10(1) doi 10.1038/s41467-019-09234-6.
23. Savinko TS, Morrison VL, Uotila LM, Wolff CHJ, Alenius HT, Fagerholm SC. Functional Beta2-Integrins Restrict Skin InflammationIn Vivo. Journal of Investigative Dermatology **2015**;135:2249-57 doi 10.1038/jid.2015.164.
24. Subramanian A, Tamayo P, Mootha VK, Mukherjee S, Ebert BL, Gillette MA*, et al.* Gene set enrichment analysis: A knowledge-based approach for interpreting genome-wide expression profiles. PNAS **2005**;102(43):15545–50 doi 10.1073pnas.0506580102.

25. Mootha VK, Lindgren CM, Eriksson K-F, Subramanian A, Sihag S, Lehar J*, et al.* PGC-1α-responsive genes involved in oxidative phosphorylation are coordinately downregulated in human diabetes. Nature Genetics **2003**;34(3) doi 10.1038/ng1180.
26. Bernstein BE, Mikkelsen TS, Xie X, Kamal M, Huebert DJ, Cuff J*, et al.* A Bivalent Chromatin Structure Marks Key Developmental Genes in Embryonic Stem Cells. Cell **2006**;125(2):315-26 doi 10.1016/j.cell.2006.02.041.
27. Solovei I, Wang AS, Thanisch K, Schmidt CS, Krebs S, Zwerger M*, et al.* LBR and LaminA/C Sequentially Tether Peripheral Heterochromatin and Inversely Regulate Differentiation. Cell **2013**;152(3):584-98.
28. Gawden-Bone C, West MA, Morrison VL, Edgar AJ, Millan SJM, Dill BD*, et al.* A crucial role for beta2 integrins in podosome formation, dynamics and Toll-like-receptor-signaled disassembly in dendritic cells. Journal of Cell Science **2014**;127(19):4213-24 doi 10.1242/jcs.151167.
29. Harr JC, Gonzalez-Sandoval A, Gasser SM. Histones and histone modifications in perinuclear chromatin anchoring: from yeast to man. EMBO reports **2016**;17:139-55 doi 10.15252/embr.201541809.
30. van Steensel B, Belmont AS. Lamina-Associated Domains: Links with Chromosome Architecture, Heterochromatin, and Gene Repression. Cell **2017**;169(5):780-91 doi 10.1016/j.cell.2017.04.022.
31. Swift J, Ivanovska IL, Buxboim A, Harada T, Dingal PCDP, Pinter J*, et al.* Nuclear Lamin-A Scales with Tissue Siffness and Enhances Matrix-Directed Differentiation. Science **2013**;341 doi 10.1126/science.1240104.
32. Borroni AP, Emanuelli A, Shah PA, Ilić N, Apel-Sarid L, Paolini B*, et al.* Smurf2 regulates stability and the autophagic–lysosomal turnover of lamin A and its disease-associated form progerin. Aging Cell **2018**;17(2):e12732 doi 10.1111/acel.12732.
33. Cytlak U, Resteu A, Bogaert D, Kuehn HS, Altmann T, Gennery A*, et al.* Ikaros family zinc finger 1 regulates dendritic cell development and function in humans nature communications **2018**;9(1) doi 10.1038/s41467-018-02977-8.
34. Boutboul D, Kuehn HS, Wyngaert ZVd, Niemela JE, Callebaut I, Stoddard J*, et al.* Dominant-negative IKZF1 mutations cause a T, B, and myeloid cell combined immunodeficiency Journal of Clinical Investigation **2018**;128(7):3071-87 doi 10.1172/JCI98164.
35. Chopin M, Lun AT, Zhan Y, Schreuder J, Coughlan H, D'Amico A*, et al.* Transcription Factor PU.1 Promotes Conventional Dendritic Cell Identity and Function via Induction of Transcriptional Regulator DC-SCRIPT. Immunity **2019**;50:77-90 doi 10.1016/j.immuni.2018.11.010.
36. Zarnegar MA, Rothenberg EV. Ikaros represses and activates PU.1 cell-type-specifically through the multifunctional Sfpi1 URE and a myeloid specific enhancer Oncogene **2013**;31(43):4647-54 doi 10.1038/onc.2011.597.
37. Krönke J, Udeshi ND, Narla A, Grauman P, Hurst SN, McConkey M*, et al.* Lenalidomide causes selective degradation of IKZF1 and IKZF3 in multiple myeloma cells Science **2014**;343(6168):301-5 doi 10.1126/science.1244851.
38. Baratin M, Foray C, Demaria O, Habbeddine M, Pollet E, Maurizio J*, et al.* Homeostatic NF-κB Signaling in Steady-State Migratory Dendritic Cells Regulates Immune Homeostasis and Tolerance. Immunity **2015**;42:627-39 doi 10.1016/j.immuni.2015.03.003.
39. Oh K-S, Gottschalk RA, Lounsbury NW, Sun J, Dorrington MG, Baek S*, et al.* Dual Roles for Ikaros in Regulation of Macrophage Chromatin State and Inflammatory Gene Expression Journal of Immmunology **2018**;201(2):757-71 doi 10.4049/jimmunol.1800158
40. Garber M, Yosef N, Goren A, Raychowdhury R, Thielke A, Guttman M*, et al.* A high-throughput chromatin immunoprecipitation approach reveals principles of dynamic gene regulation in mammals. Molecular Cell **2012**;47(5):810-22 doi 10.1016/j.molcel.2012.07.030.
41. Han H, Cho J-W, Lee S, Yun A, Kim H, Bae D*, et al.* TRRUST v2: an expanded reference database of human and mouse transcriptional regulatory interactions. Nucleic Acids Research **2018**;46(D1):D380–D6 doi 10.1093/nar/gkx1013.

42. Kidder BL, Hu G, Zhao K. KDM5B focuses H3K4 methylation near promoters and enhancers during embryonic stem cell self-renewal and differentiation. Genome Biology **2014**;15(2) doi 10.1186/gb-2014-15-2-r32.
43. Gallucci S, Lolkema M, Matzinger P. Natural adjuvants: Endogenous activators of dendritic cells. Nature Medicine **1999**;5(11):1249-55 doi 10.1038/15200.
44. Cho S, Irianto J, Discher DE. Mechanosensing by the nucleus: From pathways to scaling relationships. J Cell Biol **2017**;216(2):305-15 doi 10.1083/jcb.201610042.
45. Naetar N, Ferraioli S, Foisner R. Lamins in the nuclear interior - life outside the lamina. Journal of Cell Science **2017**;130:2087-96 doi 10.1242/jcs.203430.
46. Varga G, Balkow S, Wild MK, Stadtbaeumer A, Krummen M, Rothoeft T*, et al.* Active MAC-1 (CD11b/CD18) on DCs inhibits full T-cell activation. Blood **2007**;109(2):661-9 doi blood-2005-12-023044 [pii]

10.1182/blood-2005-12-023044.
47. Ehirchiou D, Xiong Y, Xu G, Chen W, Shi Y, Zhang L. CD11b facilitates the development of peripheral tolerance by suppressing Th17 differentiation. J Exp Med **2007**;204(7):1519-24 doi 10.1084/jem.20062292.
48. Savinko TS, Morrison VL, Uotila LM, Wolff CHJ, Alenius HT, Fagerholm SC. Functional Beta2-Integrins Restrict Skin Inflammation In Vivo. J Invest Dermatol **2015**;135(9):2249-57 doi 10.1038/jid.2015.164.
49. Han C, Jin J, Xu S, Liu H, Li N, Cao X. Integrin CD11b negatively regulates TLR-triggered inflammatory responses by activating Syk and promoting degradation of MyD88 and TRIF via Cbl-b. Nat Immunol **2010**;11(8):734-42 doi 10.1038/ni.1908.
50. Leon F, Contractor N, Fuss I, Marth T, Lahey E, Iwaki S*, et al.* Antibodies to complement receptor 3 treat established inflammation in murine models of colitis and a novel model of psoriasiform dermatitis. J Immunol **2006**;177(10):6974-82 doi 177/10/6974 [pii].
51. Haasken S, Auger JL, Binstadt BA. Absence of beta2 integrins impairs regulatory T cells and exacerbates CD4+ T cell-dependent autoimmune carditis. J Immunol **2011**;187(5):2702-10 doi 10.4049/jimmunol.1000967.
52. D'Agata ID, Paradis K, Chad Z, Bonny Y, Seidman E. Leucocyte adhesion deficiency presenting as a chronic ileocolitis. Gut **1996**;39(4):605-8.
53. Cohen SJ, Gurevich I, Feigelson SW, Petrovich E, Moser M, Shakhar G*, et al.* The integrin co-activator Kindlin-3 is not required for lymphocyte diapedesis. Blood **2013** doi 10.1182/blood-2013-04-495036.
54. Morrison VL, James MJ, Grzes K, Cook P, Glass DG, Savinko T*, et al.* Loss of beta2-integrin-mediated cytoskeletal linkage reprogrammes dendritic cells to a mature migratory phenotype. Nature communications **2014**;5:5359 doi 10.1038/ncomms6359.
55. Guenther C, Faisal I, Uotila LM, Asens ML, Harjunpää H, Savinko T*, et al.* A β2-integrin/MRTF-A/SRF Pathway Regulates Dendritic Cell Gene Expression, Adhesion, and Traction Force Generation. Frontiers in Immunology **2019**;10 doi 10.3389/fimmu.2019.01138.
56. Feit H, Kawai M, Mostafapour S. The role of collagen crosslinking in the increased stiffness of avian dystrophic muscle. Muscle & Nerve **1989**;12(6):486-92 doi 10.1002/mus.880120609.
57. Winzler C, Rovere P, Rescigno M, Granucci F, Penna G, Adorini L*, et al.* Maturation Stages of Mouse Dendritic Cells in Growth Factor–dependent Long-Term Cultures. Journal of Experimental Medicine **1997**;185(2):317-28 doi 10.1084/jem.185.2.317.
58. Miller JC, Brown BD, Shay T, Gautier EL, Jojic V, Cohain A*, et al.* Deciphering the transcriptional network of the dendritic cell lineage. nature Immunology **2012**;13:888-99 doi 10.1038/ni.2370.

Table 1

TF cluster	total tfbs	KI mean score	KI bound	WT mean score	WT bound	KI WT p value
C_IKZF1	3338	0,1518	978	0,1178	734	1,85E-54
C_SPI1	2454,2	0,1775	799	0,1408	616,8667	2,15E-10
C_SPIC	2202	0,1628	702	0,1266	534	2,89E-40
C_EWSR1-FLI1	3114	0,1185	684	0,0922	527	7,93E-17
C_Stat2	3034	0,1209	683	0,09	468	6,50E-54

Table 1: A mechanically regulated Ikaros network in DCs. (paired with Figure 5)

a) TF binding occupancy assessed by TOBIAS. Shown are top five TFs sorted by number of binding occupancies in β2-integrin KI cells.

Figure Legends

Figure 1: Inactivating β2-integrins in DCs results in increased DC maturation, IL-12 production, migration and DC-mediated tumor rejection

a) Expression of CD40, CD80 and CD86 (mean fluorescence intensity [MFI]) and CCR7 (expressed as fold change compared to WT expression) in WT and β2-integrin KI BM-DC was measured by flow cytometry; N=5. **b)** IL-12 (p40) cytokine production by WT and β2-integrin KI BMDC was measured by ELISA; N=3 **c)** WT and β2-integrin KI DC 3D; migration speed in the presence of a CCL19 gradient was assessed as described in Materials and Methods. N=3, Mann-Whitney test was used **d)** Growth of B16.OVA melanoma tumors after peritumoral injection of PBS "MOCK", β2-integrin KI DCs (KI) and WT DCs (WT). Tumor growth was measured every two days. Eight mice per group. **e)** OVA-specific infiltrating $CD8^+$ T cells in tumours (left), spleen (middle) and draining lymph nodes (right) of the animals were measured by flow cytometry. **f-g)** B16-F10 melanoma tumor growth after MOCK, β2 integrin KI DC (KI) and WT DC (WT) peritumoral injection. Tumor growth was measured every second day. Eight mice per group. **f)** Average tumor growth per group. **g)** Individual tumor volumes for each group. **h)** Number of $CD8^+$ T cells in tumors, mean +-SEM is shown **i)** number of activated $CD69^+$ $CD8^+$ T cells relative to tumor volume, mean +-SEM is shown. All p-values are shown as <0.05 *, <0.01 **, <0.005 ***,<0.0001 **** and are based on T-tests (a and b) and two way ANOVA tests (d-f). All experiments except tumor experiments were done in at least two independent experiments, error bars represent SEM

Figure 2: Inactivating β2-integrins results in an increase of H3K4me3 and H3K27me3 histone methylation marks in BM-DCs.

a) Average CTCF of H3K4me3 in WT and β2-integrin KI DCs. N=3 **b)** Example immunofluorescence picture of WT and β2-integrin KI DCs stained for H3K4me3. **c)** Example immunofluorescence picture of WT and β2-integrin KI DC nuclei stained with DAPI. **d)** Average CTCF of H3K27me3 in WT and β2-integrin KI DCs. N=3 **e)** Example immunofluorescence picture of WT and β2-integrin KI DCs stained for H3K27me3. **f)** Example immunofluorescence picture of WT and β2-integrin KI DC nuclei stained with DAPI. **g)** Western blot of H3K4me3 and H3K27me3 from WT and β2-integrin KI DCs and Western blot of Akt as control for protein loading. **h)** Average CTCF of phosphorylated RNA polymerase II (Pol II) of β2-integrin KI and WT cells. N=3. All p-values are shown as <0.05 *, <0.01 **, <0.005 ***, <0.0001 **** and are based on T-tests. All experiments were done in at least three independent experiments, error bars represent SEM

Figure 3: Disrupting adhesion, the actin cytoskeleton in WT DCs or β2-integrin/actin/lamin crosstalk results DC maturation and changes in histone methylation.

a) Expression of CD80, **b)** concentration of IL-12 (p40) and **c)** CTCF of H3K4me3 for adherent WT DCs compared with WT DCs in suspension. **d)** Average 3D migration speeds in the presence of CCL19, of DCs incubated in suspension overnight and control DCs over the time course of 4h. N=4. **e)** Average CTCF of H3K4me3, H3K27me3 and phosphorylated Pol II in β2-integrin KI DCs cultured on uncoated or fibronectin-coated coverslips. N=3 **f)** Average CTCF of H3K4me3 and H3K27me3 in β2-integrin KI DCs cultured on uncoated or fibrinogen-coated coverslips. N=3 **g)** CD40, CD80 and CD86 expression (MFI) of WT and cytochalasin D treated WT DCs was assessed by flow cytometry. N=4 **h)** Average CTCF of H3K4me3 and H3K27me3 in WT and WT cytochalasin D treated DCs. N=3. **i)** Average CTCF of lamin A/C in WT and β2-integrin KI DCs. N=3 **j)** Average CTCF of lamin B in WT and β2-integrin KI DCs. N=4 **k)** Average CTCF of H3K4me3 of WT

DCs on iC3b-coated hydrogels with 0,87kPa or 11kPa stiffness. **l)** Transcription counts of *Lmna* of WT and β2-integrin KI DCs, derived from RNA seq. data. N=3 mean +-SEM is shown. **m)** Average CTCF of Lamin A/C in non-treated WT and β2-integrin KI DCs, and in bafilomycin and MG132 treated β2-integrin KI DCs. N=3 **n)** Average CTCF of H3K4me3 and H3K27me3 in lamin A/C knockout and control DCs. N=2 **o+p)** CD80 and CCR7 expression (MFI) of HL-60 control cells, transfected with a control plasmid, and lamin overexpressing (L-AOE) HL-60. All p-values are shown as <0.05 *, <0.01 **, <0.005 ***, <0.0001 **** and are based on T-tests. All experiments were done in at least two independent experiments, error bars represent SEM

Figure 4: Increased H3K4me3 and chromatin accessibility on genes upregulated in β2-integrin KI DCs

a) Heatmap showing the coverage for histone H3K4me3 across 8 kb centered at the transcription start sites (TSS) of each RefSeq gene, standardized and segmented into 200 bins and sorted according to normalized read count (NRC) at the indicated regions in WT and β2-integrin KI DCs. **b)** Venn diagram showing the overlap between genes having elevated H3K4me3 peaks at their promoter region (-3kb to +5kb from the TSS) in β2-integrin KI cells (at least 50% difference from WT) versus genes displaying increased expression in β2-integrin KI cells (RNAseq data) **c)-h)** RNA-Seq, ATAC-Seq and H3K4me3 ChIP-Seq tracks at the coding regions of **c)** *Cd40*, **d)** *Cd80*, **e)** *Cd86*, **f)** *Il-12b*, **g)** *Ccr7* and **h)** *Fscn1*.

Figure 5: A mechanically responsive Ikaros (IKZF1)/NF-kB regulated gene network in β2-integrin KI DCs drives the mature, migratory phenotype.

a) Comparison of Ikaros-regulated (activated) genes with the β2-integrin KI upregulated genes. Here, the Ikaros-regulated genes are taken from (39) and the β2-integrin KI upregulated genes are based on RNA-Seq expression data (previously published (8), re-analyzed, Supplementary Table 3). GO-analysis results of the 100 intersecting genes are listed. **b)** Venn diagram of PU.1 activated genes(35) and genes upregulated at least two folds based on β2-integrin KI DC RNA-Seq data. GO-analysis results of the 100 intersecting genes are listed. **c)** IL-12 (p40) production of non-treated (NT) and lenalidomide treated β2-integrin KI DCs was measured by ELISA. N=3 **d)** 3D migration speeds in collagen towards CCl19 of NT and lenalidomide treated β2-integrin KI DCs N=3, the mean values are indicated **e)** RelA bound genes, β2-integrin KI upregulated genes and overlapping genes based on TLR-stimulated genes in BM-DCs published in (40). **f)** Total percentages of WT and KI β2-integrin DCs with nuclear RelA and cells in which RelA was not in the nucleus are shown, N=3. **g)** Total percentages of cells with nuclear RelA and cells in which RelA was not in the nucleus from **h)** non-treated WT and WT DCs in suspension **i)** control DCs and LaminA/C KO DCs and on hydrogels with 0,87kPa, 11kPA or 90kPa stiffness. N=3. All p-values are shown as <0.05 *, <0.01 ** and are based on T-test for c and Mann-Whitney test for d. All experiments were done in at least two independent experiments, error bars represent SEM

Figure 6: Inhibiting histone demethylation stabilizes the suspension treatment effect on WT DCs and results in improved antitumor responses *in vivo*

a) H3K4me3 and H3K4me2 on *Ccr7* of WT NT and WT TCP-treated DCs. **b)** Fold changes of CCR7 mRNA in WT TCP-treated and WT TCP+suspension cells was assessed by qPCR. mRNA level of WT NT was set to 1 and used as base line. (N=3) **c)** Expression of CD86 (N=4). **d)** IL-12 (p40) production (N=3) and **e)** 3D migration speed following TCP treatment on adherent WT DCs and WT DCs in suspension N=3. p=value for WT NT vs WT TCP+susp. is 0.0235. The mean values are indicated with a horizontal line. **f)** 3D migration speed of IOX-treated adherent WT DCs and non-treated adherent WT DCs N=2.

p=value is 0.0059. The mean values are indicated with a horizontal line. **g)** 3D migration speed of control and $CCR7^{-/-}$ DCs (CCR7 KO) following TCP and suspension treatment N=3. The mean values are indicated with a horizontal line. h**)** Tumor growth following PBS injection (MOCK), WT NT, or β2-integrin KI DC injection as well as injection with TCP-treated WT DCs in suspension. i**)** Tumor growth following injection with: PBS (MOCK), or CCR7 KO DCs or WT DCs treated with TCP and suspension. All p-values are shown as <0.05 *, <0.01 **, <0.005 ***, <0.0001 **** and are based on T-tests (b-d), Mann-Whitney test (e-g) and two-way ANOVA (h, i). All experiments were done in at least two independent experiments, error bars represent SEM

Figure 1

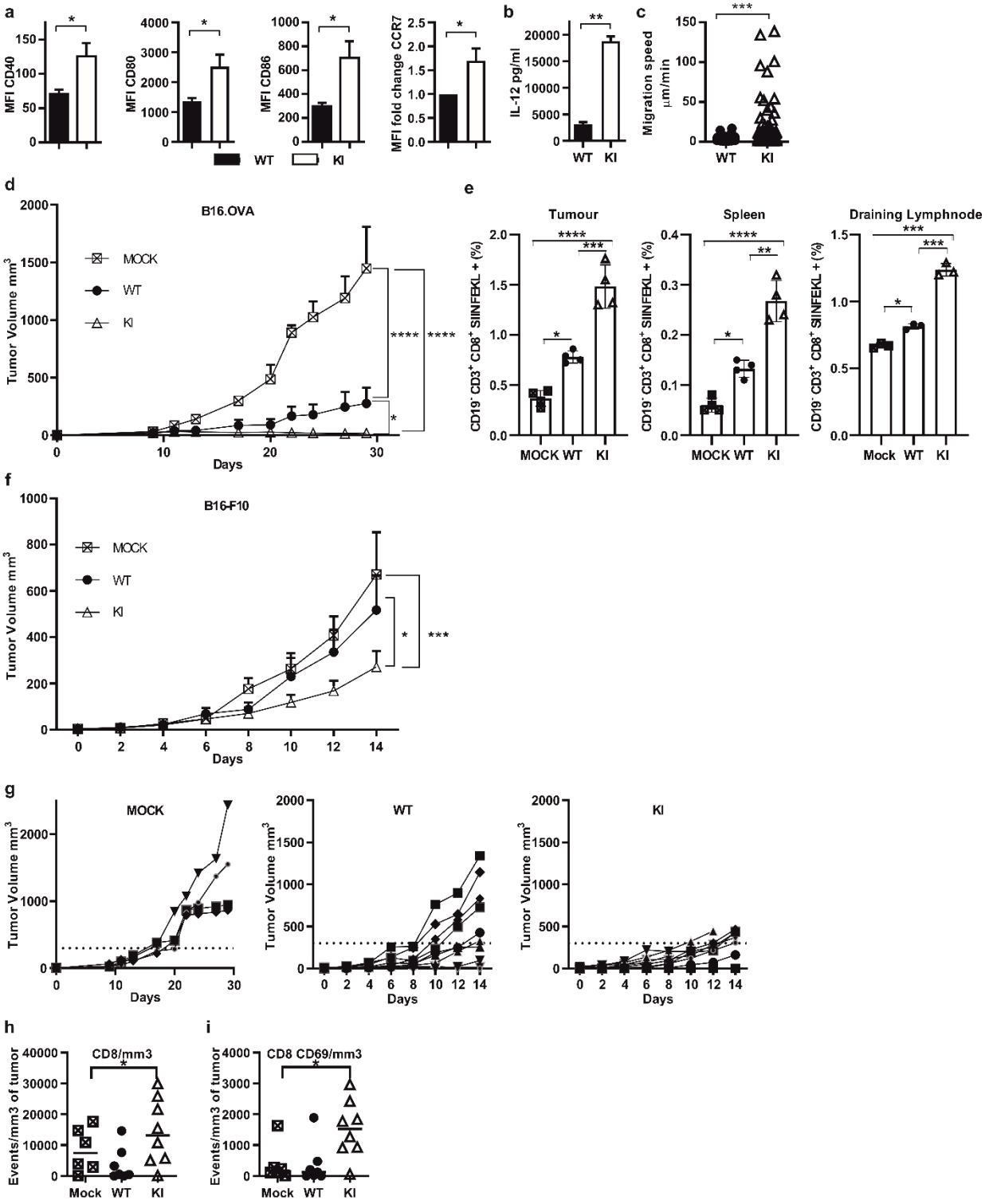
a
MFI CD40
MFI CD80
MFI CD86
MFI fold change CCR7
WT
KI
b
IL-12 pg/ml
c
Migration speed µm/min
d
B16.OVA
MOCK
WT
KI
Tumor Volume mm3
Days
e
Tumour
Spleen
Draining Lymphnode
CD19- CD3+ CD8+ SIINFEKL + (%)
MOCK WT KI
Mock WT KI
f
B16-F10
g
MOCK
WT
KI
h
CD8/mm3
Events/mm3 of tumor
i
CD8 CD69/mm3

Figure 2

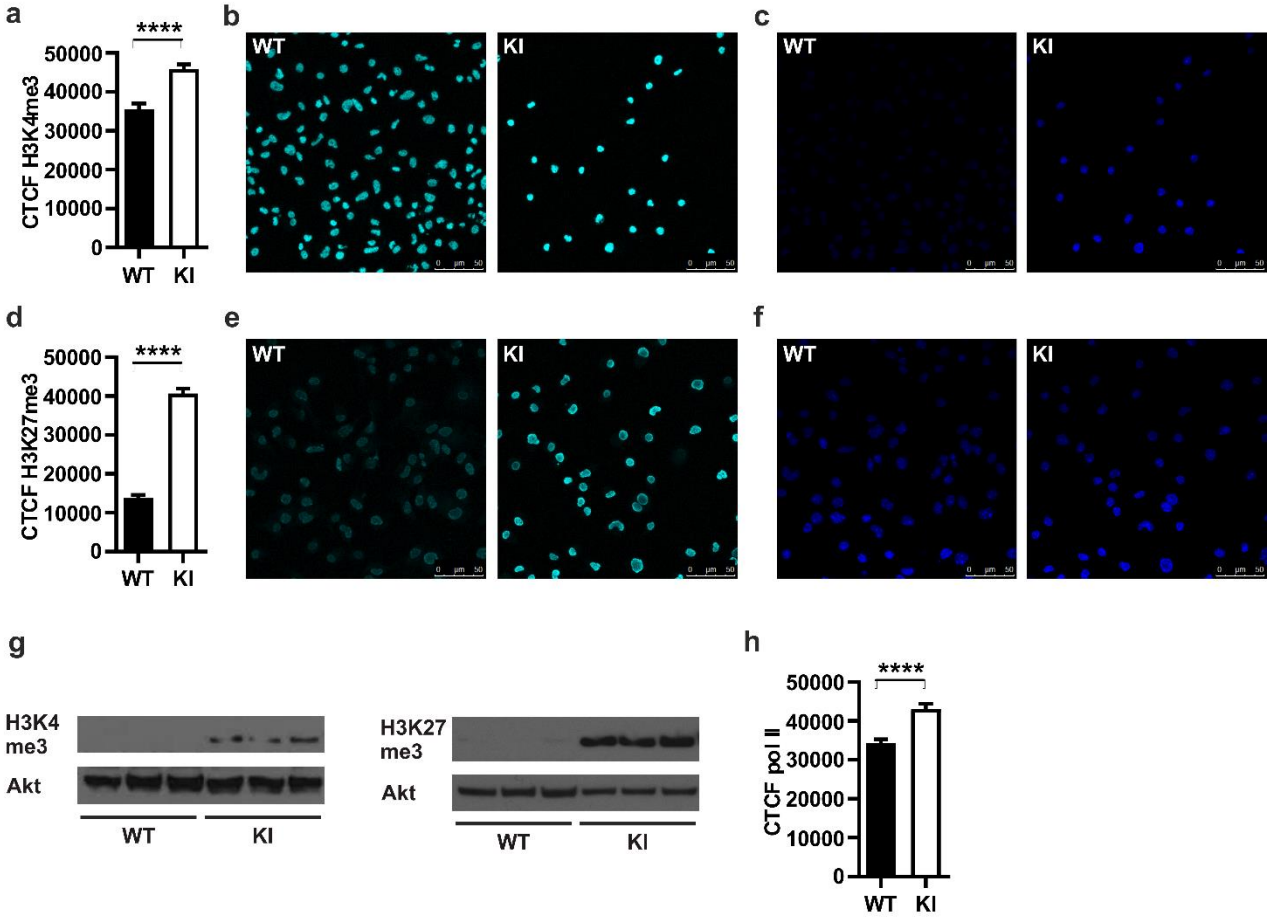
a
****
CTCF H3K4me3
50000
40000
30000
20000
10000
0
WT
KI
b
WT
KI
c
WT
KI
d
****
CTCF H3K27me3
50000
40000
30000
20000
10000
0
WT
KI
e
WT
KI
f
WT
KI
g
H3K4 me3
Akt
WT
KI
H3K27 me3
Akt
WT
KI
h
****
CTCF pol II
50000
40000
30000
20000
10000
0
WT
KI

Figure 3

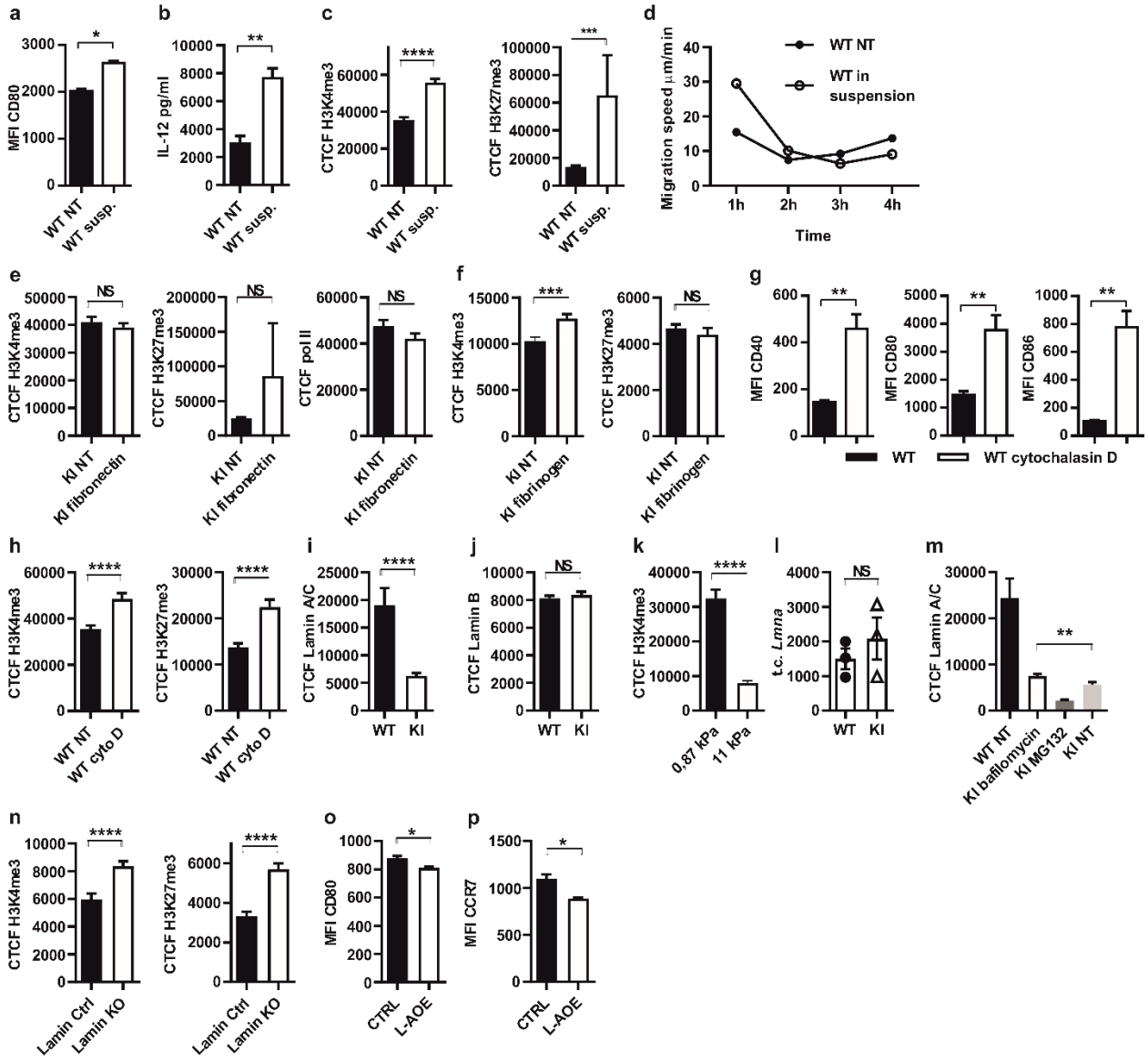
a
MFI CD80
WT NT
WT susp.
b
IL-12 pg/ml
c
CTCF H3K4me3
CTCF H3K27me3
d
Migration speed µm/min
WT NT
WT in suspension
1h
2h
3h
4h
Time
e
CTCF H3K4me3
CTCF H3K27me3
CTCF pol II
KI NT
KI fibronectin
NS
f
KI fibrinogen
g
MFI CD40
MFI CD80
MFI CD86
WT
WT cytochalasin D
h
WT cyto D
i
CTCF Lamin A/C
WT
KI
j
CTCF Lamin B
k
0,87 kPa
11 kPa
l
t.c. Lmna
m
KI bafilomycin
KI MG132
n
Lamin Ctrl
Lamin KO
o
CTRL
L-AOE
p
MFI CCR7

Figure 4

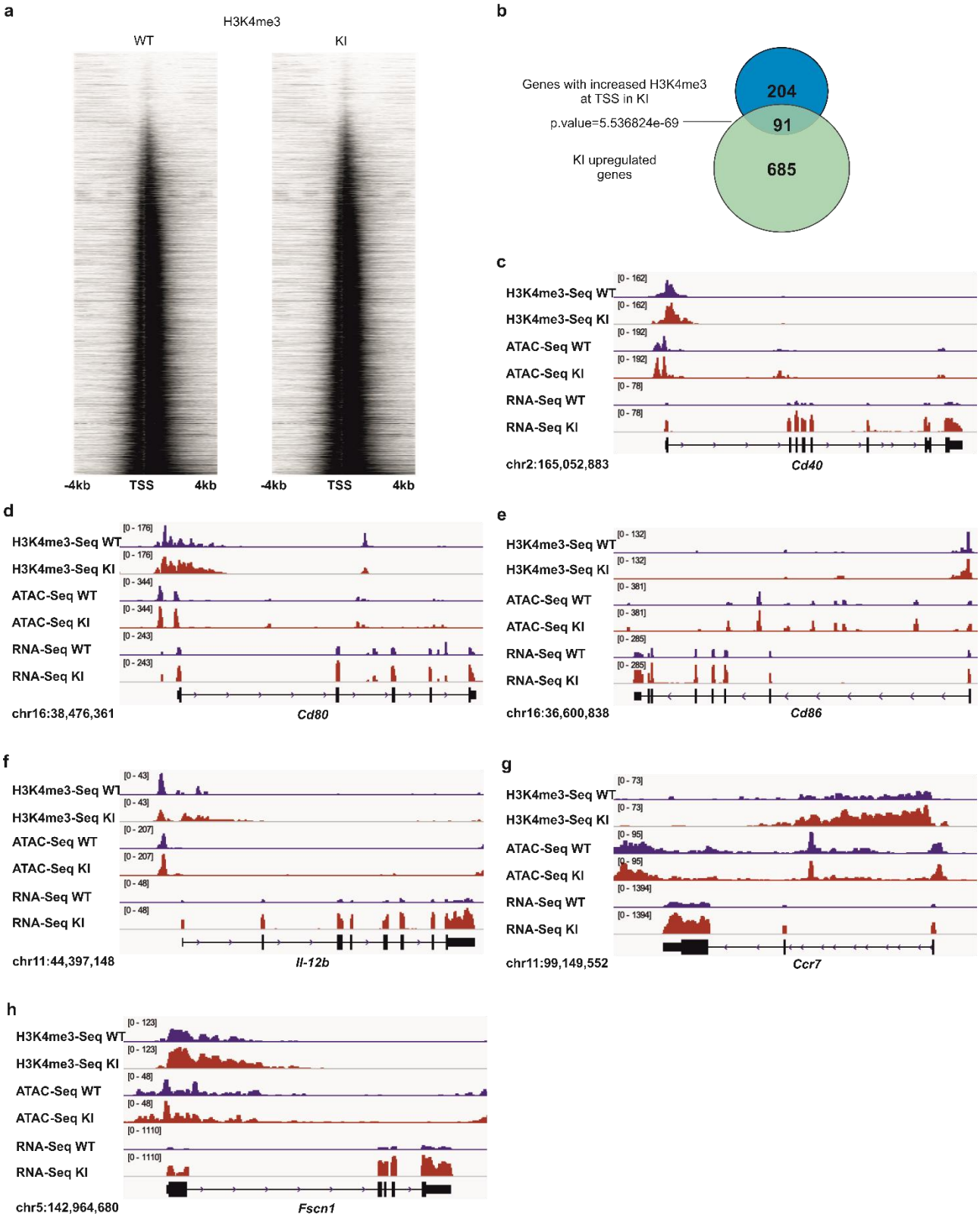
a
H3K4me3
WT
KI
-4kb
TSS
4kb
-4kb
TSS
4kb
b
Genes with increased H3K4me3 at TSS in KI
p.value=5.536824e-69
KI upregulated genes
204
91
685
c
H3K4me3-Seq WT
H3K4me3-Seq KI
ATAC-Seq WT
ATAC-Seq KI
RNA-Seq WT
RNA-Seq KI
chr2:165,052,883
Cd40
d
H3K4me3-Seq WT
H3K4me3-Seq KI
ATAC-Seq WT
ATAC-Seq KI
RNA-Seq WT
RNA-Seq KI
chr16:38,476,361
Cd80
e
H3K4me3-Seq WT
H3K4me3-Seq KI
ATAC-Seq WT
ATAC-Seq KI
RNA-Seq WT
RNA-Seq KI
chr16:36,600,838
Cd86
f
H3K4me3-Seq WT
H3K4me3-Seq KI
ATAC-Seq WT
ATAC-Seq KI
RNA-Seq WT
RNA-Seq KI
chr11:44,397,148
Il-12b
g
H3K4me3-Seq WT
H3K4me3-Seq KI
ATAC-Seq WT
ATAC-Seq KI
RNA-Seq WT
RNA-Seq KI
chr11:99,149,552
Ccr7
h
H3K4me3-Seq WT
H3K4me3-Seq KI
ATAC-Seq WT
ATAC-Seq KI
RNA-Seq WT
RNA-Seq KI
chr5:142,964,680
Fscn1